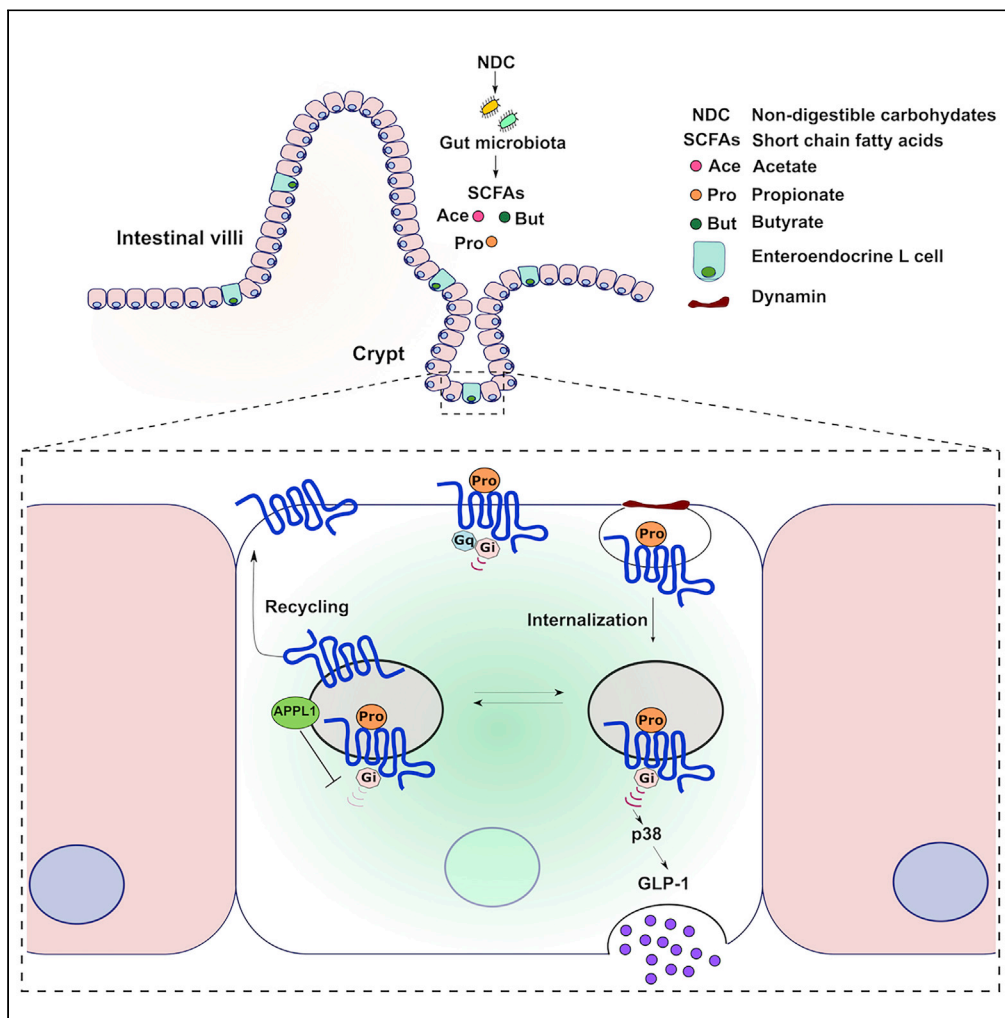


Article

# Internalization-Dependent Free Fatty Acid Receptor 2 Signaling Is Essential for Propionate-Induced Anorectic Gut Hormone Release



Natarin  
Caengprasath,  
Noemi Gonzalez-  
Abuin, Maria  
Shchepinova, ...,  
Edward W. Tate,  
Gary Frost, Aylin  
C. Hanyaloglu

a.hanyaloglu@imperial.ac.uk

**HIGHLIGHTS**

Propionate activates *Gai/o* but no *Gαq/11* signaling in STC-1 cells or colonic crypts

Acute *Gai/o* signaling via FFA2 requires endocytosis and mediates GLP-1 release

FFA2 traffics to very early endosomes to control rapid recycling and *Gai/o* signals

Propionate-induced internalization of FFA2 drives p38 signaling and GLP-1 release



## Article

## Internalization-Dependent Free Fatty Acid Receptor 2 Signaling Is Essential for Propionate-Induced Anorectic Gut Hormone Release

Natarin Caengprasath,<sup>1,6</sup> Noemi Gonzalez-Abuin,<sup>2,6</sup> Maria Shchepinova,<sup>3</sup> Yue Ma,<sup>2</sup> Asuka Inoue,<sup>4</sup> Edward W. Tate,<sup>3</sup> Gary Frost,<sup>2,5</sup> and Aylin C. Hanyaloglu<sup>1,5,7,\*</sup>

## SUMMARY

The ability of propionate, a short-chain fatty acid produced from the fermentation of non-digestible carbohydrates in the colon, to stimulate the release of anorectic gut hormones, such as glucagon like peptide-1 (GLP-1), is an attractive approach to enhance appetite regulation, weight management, and glycemic control. Propionate induces GLP-1 release via its G protein-coupled receptor (GPCR), free fatty acid receptor 2 (FFA2), a GPCR that activates  $G\alpha_i$  and  $G\alpha_q/11$ . However, how pleiotropic GPCR signaling mechanisms in the gut regulates appetite is poorly understood. Here, we identify propionate-mediated G protein signaling is spatially directed within the cell whereby FFA2 is targeted to very early endosomes. Furthermore, propionate activates a  $G\alpha_i/p38$  signaling pathway, which requires receptor internalization and is essential for propionate-induced GLP-1 release in enteroendocrine cells and colonic crypts. Our study reveals that intestinal metabolites engage membrane trafficking pathways and that receptor internalization could orchestrate complex GPCR pathways within the gut.

## INTRODUCTION

The consumption of dietary fiber, or non-digestible carbohydrates (NDCs), has been shown to protect against diet-induced obesity (Chambers et al., 2015). The protective effects of NDCs are largely attributed to short-chain fatty acids (SCFAs) that are produced in the colon by microbiota from the fermentation of NDCs (Chambers et al., 2015; Den Besten et al., 2013; James et al., 2003). Acetate, propionate, and butyrate are the predominant SCFAs produced and, in addition to regulation of gastro-intestinal functions, are involved in energy and glucose homeostasis and immune responses (Den Besten et al., 2013). Traditionally, roles of SCFAs in these metabolic processes were thought to be limited to their ability to act as an energy source or as a regulator of cholesterol synthesis; however, with the discovery and characterization of G protein-coupled receptors (GPCRs) activated by SCFAs, free fatty acid receptor 2 (FFA2, previously known as GPR43) and free fatty acid receptor 3 (FFA3, previously known as GPR41), it is now widely appreciated that many SCFA activities can be attributed to these receptors (Fuller et al., 2015; Li et al., 2018; Pingitore et al., 2019; Tolhurst et al., 2012; Bolognini et al., 2016).

Among the three SCFAs, propionate has been of particular translational interest owing to its ability to acutely suppress appetite via activation of FFA2 in enteroendocrine L cells and release of the anorectic gut hormones peptide YY (PYY) and incretin glucagon like peptide-1 (GLP-1) (Tolhurst et al., 2012; Psichas et al., 2015), contributing to its role in rapid weight loss and improved insulin sensitivity following Roux-en-Y gastric bypass (Liou et al., 2013). Direct health benefits of propionate in humans have been recently demonstrated whereby increasing the colonic levels of propionate in overweight humans not only exhibited reduced weight gain but also reduced abdominal adiposity and improved insulin sensitivity (Chambers et al., 2015). Thus propionate, and its receptor-mediated actions, represents an attractive system to develop therapeutic strategies in obesity management.

Although the role of SCFAs and their receptors in mediating the release of anorectic gut hormones has been demonstrated in rodent models and humans (Tolhurst et al., 2012; Bolognini et al., 2016; Psichas et al., 2015; Chambers et al., 2015), our understanding of the molecular mechanisms by propionate,

<sup>1</sup>Institute of Reproductive and Developmental Biology (IRDB), Department of Metabolism, Digestion and Reproduction, Imperial College London, Rm 2009, Hammersmith Campus, Du Cane Road, London W12 0NN, UK

<sup>2</sup>Department of Metabolism, Digestion and Reproduction, Imperial College London, London, UK

<sup>3</sup>Department of Chemistry, Imperial College London, London, UK

<sup>4</sup>Graduate School of Pharmaceutical Sciences, Tohoku University, Sendai, Japan

<sup>5</sup>Senior author

<sup>6</sup>These authors contributed equally

<sup>7</sup>Lead Contact

\*Correspondence: a.hanyaloglu@imperial.ac.uk  
<https://doi.org/10.1016/j.isci.2020.101449>



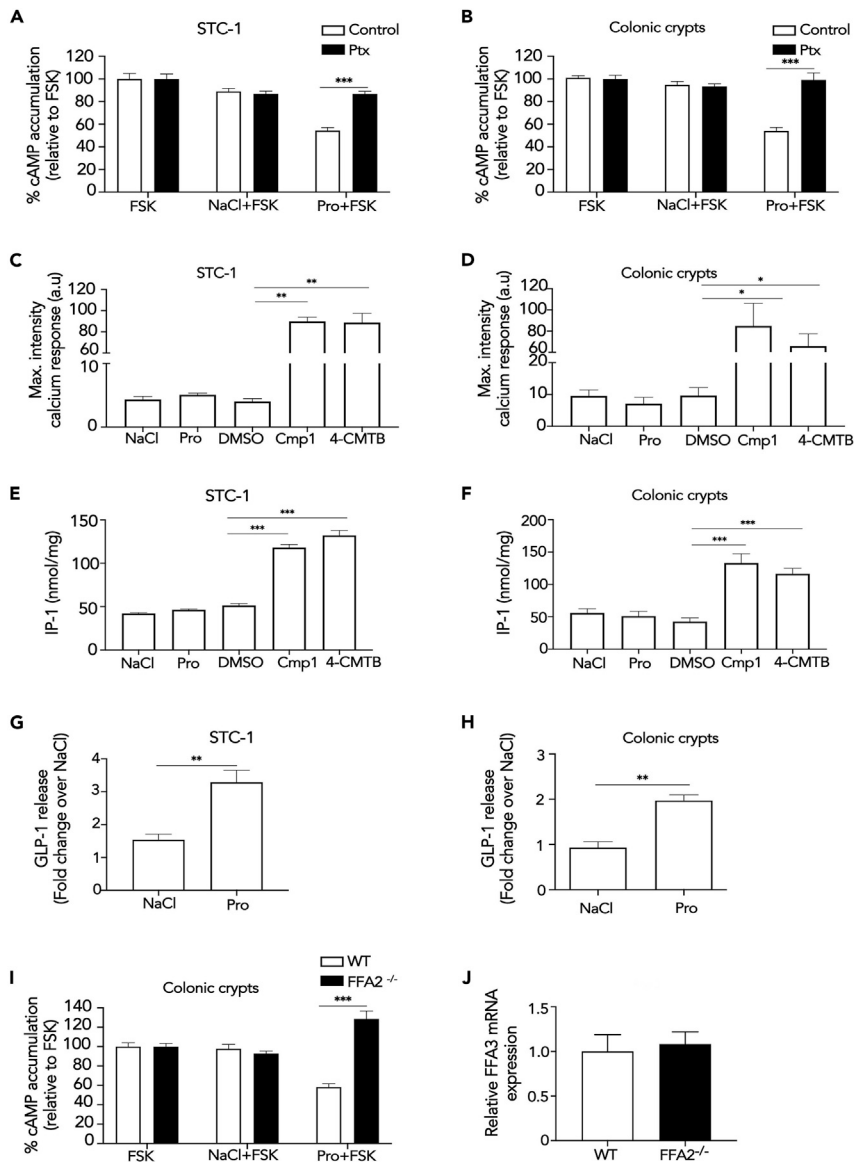


**Figure 1. Propionate Stimulates GLP-1 Secretion and Activates *Gxi/o* but Not *Gαq/11* via FFA2**

(A and B) Intracellular cAMP levels measured in STC-1 cells (A) or colonic crypts (B) pre-treated with Pertussis toxin (Ptx; 200 ng/mL, 20 h) prior to pre-treatment with IBMX (0.5 mM, 5 min) and then stimulated with forskolin (FSK, 3 μM) or a combination of FSK with either NaCl or sodium propionate (Pro) (1 mM, 5 min). Data are expressed as percent change of FSK-treated cells. n = 3 independent experiments. Two-sided Mann-Whitney U test, \*\*\*p < 0.001.

(C and D) Intracellular calcium mobilization measured in STC-1 cells (C) or colonic crypts (D). Cultures were incubated with calcium indicator Fluo4-AM for 1 h and imaged live via confocal microscopy for 1 min before the addition of NaCl (1 mM), sodium propionate (Pro), DMSO, orthosteric FFA2 agonist Cmp1 (10 μM), or allosteric FFA2 agonist 4-CMTB (10 μM). Average maximal intensities of n = 20 cells in duplicate per six independent experiments. Two-sided Mann-Whitney U test, \*p < 0.05.

(E and F) Intracellular accumulation of IP<sub>1</sub> in STC-1 cells (E) or colonic crypts (F). Cultures were treated with NaCl, sodium propionate (Pro) (1 mM), DMSO, Cmp1 (10 μM), or 4-CMTB (10 μM) for 2 h. STC-1 cells or crypts, n = 3 independent experiments. Two-sided Mann-Whitney U test, \*\*\*p < 0.001. Data represent mean ± SEM.

(G and H) (G) STC-1 cells and (H) colonic crypts were treated with either NaCl or sodium propionate (Pro) (1 mM, 2 h STC-1, 1 h crypts), and total GLP-1 levels secreted were measured via RIA. Data are expressed as fold change of total GLP-1 and normalized to basal (NaCl) secretion within the same experiment. For STC-1 cells, n = 4 independent experiments. For crypts, n = 3 independent experiments. Two-sided Mann-Whitney U test, \*p < 0.05, \*\*p < 0.01.

**Figure 1. Continued**

(I) Intracellular cAMP levels measured in colonic crypts from wild-type (WT) or FFA2 knockout mice (FFA2<sup>-/-</sup>) pre-treated with IBMX (0.5 mM, 5 min) and then stimulated as in (C) and (D). Data are expressed as percent change of FSK-treated cells. n = 3 independent experiments. Two-sided Mann-Whitney U test, \*\*\*p < 0.001.

(J) Expression levels of FFA3 in WT and FFA2<sup>-/-</sup> colonic crypts. mRNA isolated from colonic crypts of WT and FFA2<sup>-/-</sup> mice were used in qPCR studies with specific mouse FFA3 primers. Data are presented as  $\Delta\Delta\text{Ct}$ . Two-sided Mann-Whitney U test. Data represent mean  $\pm$  SEM.

See also [Figures S1–S4](#) and [Videos S1, S2, and S3](#).

regulating the release of anorectic gut hormone from enteroendocrine L cells, remains limited. FFA2 is coupled to both the *G $\alpha$ i/o* and *G $\alpha$ q/11* families of heterotrimeric G proteins (Brown et al., 2003; Le Poul et al., 2003), although *G $\alpha$ q/11* is implicated in mediating gut hormone release via increases in calcium (Bolognini et al., 2016; Tolhurst et al., 2012). Models of GPCR signaling, however, have rapidly evolved over recent years from single receptors activating distinct G protein pathways at the plasma membrane, to high signal diversity that can be differentially activated by distinct ligands and exquisitely regulated at a spatial and temporal level. The spatiotemporal regulation of GPCRs can occur via a variety of processes, with membrane trafficking of GPCRs playing a central role. Membrane trafficking of GPCRs was classically viewed as a mechanism to control active cell surface receptor number by driving receptor internalization and post-endocytic sorting to divergent cellular fates. However, it is now understood that receptor internalization to endosomes provides additional intracellular signaling platforms including activation of heterotrimeric G protein signaling (Eichel and Von Zastrow, 2018; Hanyaloglu, 2018; Calebiro et al., 2009; Ferrandon et al., 2009). Endosomal signaling of GPCRs exhibits distinct functions from signaling activated at the plasma membrane, demonstrating the integrated nature of trafficking and signaling and providing a mechanism for cells to achieve highly specific and diverse downstream responses to its dynamic extracellular environment (Thomsen et al., 2018; Caengprasath and Hanyaloglu, 2019). Furthermore, we have previously shown that GPCRs are organized to distinct endosomal compartments to activate signaling (Sposini et al., 2017; Jean-Alphonse et al., 2014). These discoveries over the past decade have rewritten the GPCR “signaling atlas,” offering new interpretations of faulty GPCR activity in disease and providing novel therapeutic strategies to target GPCR signaling (Thomsen et al., 2018). However, the role of membrane trafficking for FFA2 and the distinct actions of propionate that activates pleiotropic G protein signal pathways within the gut remain unknown.

In this study, we demonstrate internalization-dependent FFA2 signaling drives propionate-induced GLP-1 release from enteroendocrine cells. Furthermore, we provide evidence that G protein signaling activated by FFA2 is differentially regulated by membrane trafficking and that an unexpected *G $\alpha$ i/p38* signaling pathway is required for propionate-induced GLP-1 release.

**RESULTS****Propionate Stimulates GLP-1 Secretion yet Activates *G $\alpha$ i/o* but Not *G $\alpha$ q/11* Signaling from Colonic Crypts and Enteroendocrine Cells**

Although propionate is known to mediate anorectic gut hormone release via FFA2, the ability of this SCFA to activate both upstream *G $\alpha$ q/11* and *G $\alpha$ i/o* signal pathways in enteroendocrine cells has yet to be fully demonstrated. FFA2 couples to both *G $\alpha$ i/o* to inhibit adenylate cyclase and reduce intracellular levels of cAMP and *G $\alpha$ q/11* that activates phospholipase C resulting in increases in inositol 1,4,5-triphosphate (IP<sub>3</sub>) and diacylglycerol, leading to mobilization of calcium from intracellular stores.

In both mouse enteroendocrine (STC-1) cells and colonic crypts, 1 mM propionate, a physiologically relevant dose that induced maximal responses in STC-1 cells and HEK 293 cells expressing FFA2 (Figures S1A and S1B) was able to inhibit forskolin-induced cAMP, which was significantly reversed by pre-treatment with *G $\alpha$ i/o* inhibitor pertussis toxin (Ptx) (Figures 1A and 1B). Surprisingly, 1 mM propionate did not induce either an increase in intracellular calcium (Figures 1C and 1D and Video S1) or IP<sub>1</sub>, a downstream metabolite of IP<sub>3</sub>, in either STC-1 cells or colonic crypts (Figures 1E and 1F) despite its ability to induce GLP-1 release (Figures 1G and 1H). Treatment with a higher dose of propionate (10 mM) in both STC-1 cells and crypts also did not significantly increase intracellular IP<sub>1</sub> or calcium levels (Figure S2). In contrast, a previously described selective FFA2 synthetic allosteric ligand (Lee et al., 2008), 4-CTMB, and a previously characterized selective FFA2 synthetic orthosteric ligand, compound 1 (Hudson et al., 2013) (Cmp1), activated both *G $\alpha$ i/o* and *G $\alpha$ q/11* signaling in STC-1 cells and colonic crypts (Figures S1D and 1C–1F and Videos S2 and

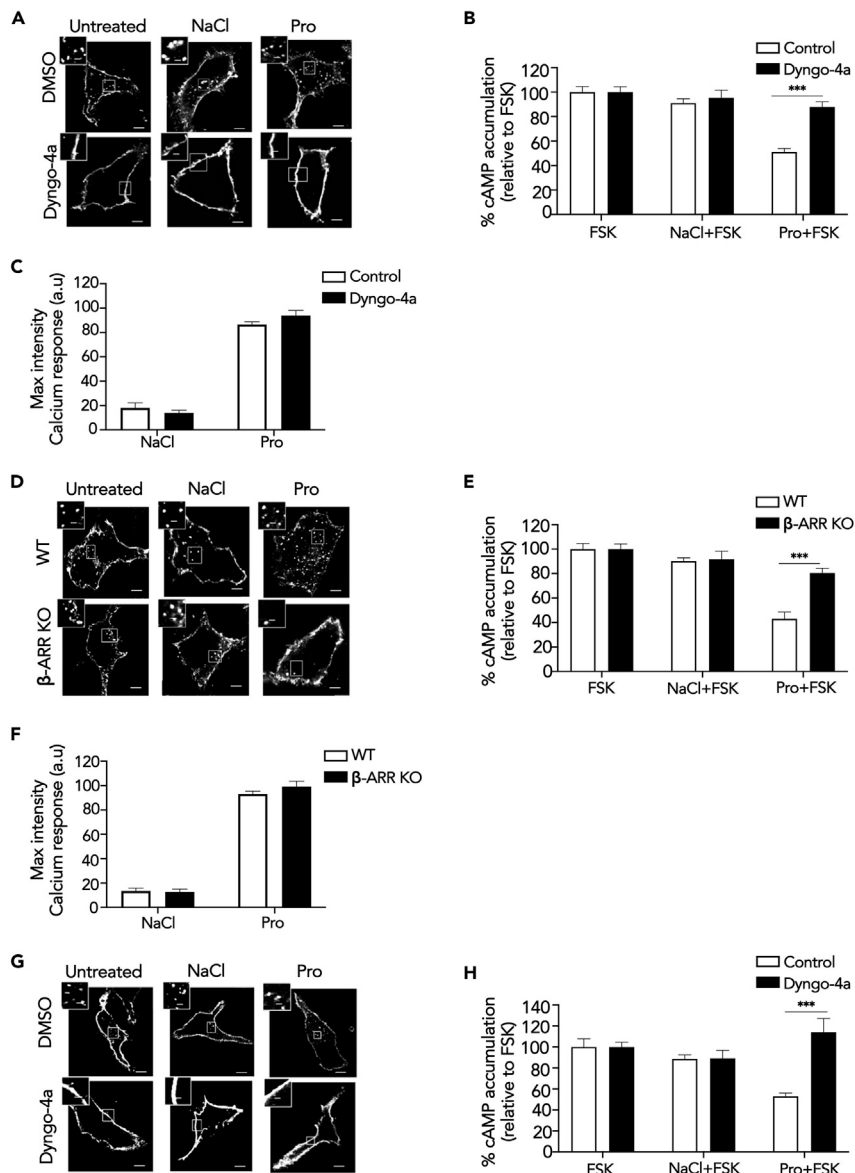


### Figure 2. Propionate-Dependent $G\alpha_i/o$ Signaling Requires Receptor Internalization

(A) Representative confocal microscopy images of HEK 293 cells expressing FLAG-FFA2 were pre-treated with either DMSO (vehicle) or Dyngo-4a (50 μM, 45 min), fed with M1 anti-FLAG antibody prior to stimulation with either NaCl or sodium propionate (Pro) (1 mM, 20 min). Fixed cells were imaged via confocal microscopy.

(B and C) Intracellular cAMP levels (B) or calcium mobilization (C) measured in HEK 293 cells expressing FLAG-FFA2 pre-treated with either DMSO (vehicle) or Dyngo-4a (50 μM, 45 min). For (B), cells were pre-treated with IBMX (0.5 mM, 5 min) and then stimulated with forskolin (FSK, 3 μM) or a combination of FSK with either NaCl or sodium propionate (Pro) (1 mM, 5 min).  $n = 3$  independent experiments. Two-sided Mann-Whitney U test, \*\*\* $p < 0.001$ . For (C), cells were incubated with calcium indicator Fluo4-AM for 1 h and imaged live via confocal microscopy for 1 min before the addition of either NaCl or sodium propionate (Pro) (1 mM). Average maximal intensities of  $n = 20$  cells in duplicate per four independent experiments.

(D) Representative confocal microscopy images of WT or β-ARR KO HEK 293 cells expressing FLAG-FFA2. Cells were treated with FLAG antibody and ligands and imaged as in (A).

(E and F) Intracellular cAMP levels (E) or calcium mobilization (F) measured in WT or β-ARR KO HEK 293 cells transiently expressing FLAG-FFA2. Samples were treated and assayed as in (B) and (C).  $n = 3$  independent experiments for either WT or β-ARR KO HEK 293 cells transiently expressing FLAG-FFA2. Two-sided Mann-Whitney U test, \*\*\* $p < 0.001$ .

(G) Representative confocal images of STC-1 cells transiently expressing FLAG-FFA2 pre-treated with either DMSO (vehicle) or Dyngo-4a (50 μM, 45 min) then stimulated as in (A).

**Figure 2. Continued**

(H) Intracellular cAMP levels of STC-1 pre-treated with either DMSO (vehicle) or Dyngo-4a (50  $\mu$ M, 45 min). Scale bar, 5  $\mu$ m; scale bar in inset, 1  $\mu$ m. n = 3 independent experiments. Two-sided Mann-Whitney U test, \*\*\*p < 0.001. For confocal images, representative images are shown of ~10 cells/experiment. Data represent mean  $\pm$  SEM. See also [Figure S5](#).

S3). Both compounds were also used at doses shown to induce maximal signal responses ([Lee et al., 2008](#); [Hudson et al., 2012](#) and [Figure S1C](#)), thus further demonstrating functional FFA2 in both cultures. The synthetic ligand-induced calcium responses were  $G\alpha q/11$  mediated as they were significantly impaired by the pre-treatment of a selective  $G\alpha q/11$  inhibitor, YM-254890 ([Takasaki et al., 2004](#)), in STC-1 cells ([Figure S3](#)).

Despite the lack of detectable  $G\alpha q/11$  signaling, propionate-induced- $G\alpha i/o$  signaling was dependent on FFA2 as the reduction of forskolin-induced cAMP in colonic crypts derived from FFA2 knockout mice (FFA2<sup>-/-</sup>) was completely abolished ([Figure 1I](#)), consistent with our prior reports from the same mouse model that propionate-induced gut hormone release from the colon requires FFA2 ([Psichas et al., 2015](#)). This loss of propionate-mediated  $G\alpha i/o$  signaling in the FFA2<sup>-/-</sup> crypts was not due to alterations in FFA3 expression ([Figure 1J](#)).

These data confirm that despite functional FFA2 responses, propionate activates  $G\alpha i/o$  signaling without detectable  $G\alpha q/11$  responses in these cultures. To determine if the inability of propionate to activate  $G\alpha q/11$  signaling via FFA2 was cellular context-specific, we stimulated HEK 293 cells expressing FLAG-FFA2. Treatment with 1 mM propionate significantly induced increases in intracellular calcium and IP<sub>1</sub> ([Figure S4](#)) confirming activation of  $G\alpha q/11$  signaling. Taken together, this demonstrates that, unlike synthetic FFA2 ligands, propionate is not able to signal via  $G\alpha q/11$  in enteroendocrine cells, suggesting additional mechanisms beyond G protein activation are employed to induce propionate-mediated anorectic gut hormone secretion.

**FFA2/G Protein Signaling Is Spatially Regulated**

We next determined if propionate/FFA2 activation is spatially regulated via membrane trafficking as a potential mechanism underlying its actions in the gut. Many GPCRs undergo ligand-induced internalization via a well-described  $\beta$ -arrestin- and clathrin-dependent mechanism, whereby the large GTPase dynamin regulates the latter steps of endocytosis that drive clathrin-coated vesicle scission. To inhibit FFA2 internalization, the ability of a potent inhibitor of dynamin GTPase activity, Dyngo-4a, known to block the internalization of many GPCRs ([Mccluskey et al., 2013](#); [Eichel et al., 2016](#); [Tsvetanova and Von Zastrow, 2014](#); [Sposini et al., 2017](#)), was first assessed in HEK 293 cells expressing FLAG-tagged FFA2 and imaged via confocal microscopy. Unexpectedly, FFA2 exhibited both constitutive and propionate-dependent internalization from the plasma membrane ([Figure 2A](#)), which was confirmed via flow cytometry ([Figure S5A](#)). In cells pre-treated with Dyngo-4a, a strong inhibition of both constitutive and propionate-induced FFA2 internalization was observed ([Figure 2A](#)), demonstrating that FFA2 constitutive and ligand-induced internalization occur in a dynamin-dependent manner. Under conditions where dynamin-dependent FFA2 internalization was inhibited in HEK 293 cells, the ability of propionate to inhibit forskolin-induced cAMP was impaired ([Figure 2B](#)). In contrast, FFA2-mediated  $G\alpha q/11$  signaling, as measured by intracellular calcium responses ([Figure 2C](#)) or IP-1 accumulation ([Figure S5B](#)), was not significantly affected, suggesting a differential requirement of FFA2 internalization for FFA2-mediated signaling. These results were also confirmed in HEK 293 cells lacking  $\beta$ -arrestins 1 and 2 ([Grundmann et al., 2018](#)) ([Figure S5C](#)). Interestingly, only ligand-induced, but not constitutive, FFA2 internalization was inhibited by lack of  $\beta$ -arrestins ([Figures 2D](#) and [S5D](#)). However, as in cells pre-treated with Dyngo-4a, propionate-dependent inhibition of forskolin-induced cAMP was significantly impaired in  $\beta$ -arrestin knockout cells compared with wild-type HEK 293 cells ([Figure 2E](#)). In contrast, propionate-induced calcium mobilization and IP<sub>1</sub> accumulation was unperurbed ([Figures 2F](#) and [S5E](#)).

The requirement of receptor internalization for  $G\alpha i/o$  signaling was also determined for the endogenous propionate-responsive receptors expressed in STC-1 cells. As specific antibodies are not available for these receptors, STC-1 cells were transfected with FLAG-tagged FFA2 to confirm required conditions to inhibit FFA2 internalization in these cells. Similar to HEK 293 cells, FFA2 internalization exhibited both constitutive and ligand-induced endocytic profiles, and both were inhibited by Dyngo-4a ([Figure 2G](#)). Consistent with our observations in HEK 293 cells, Dyngo-4a pre-treatment inhibited propionate-mediated



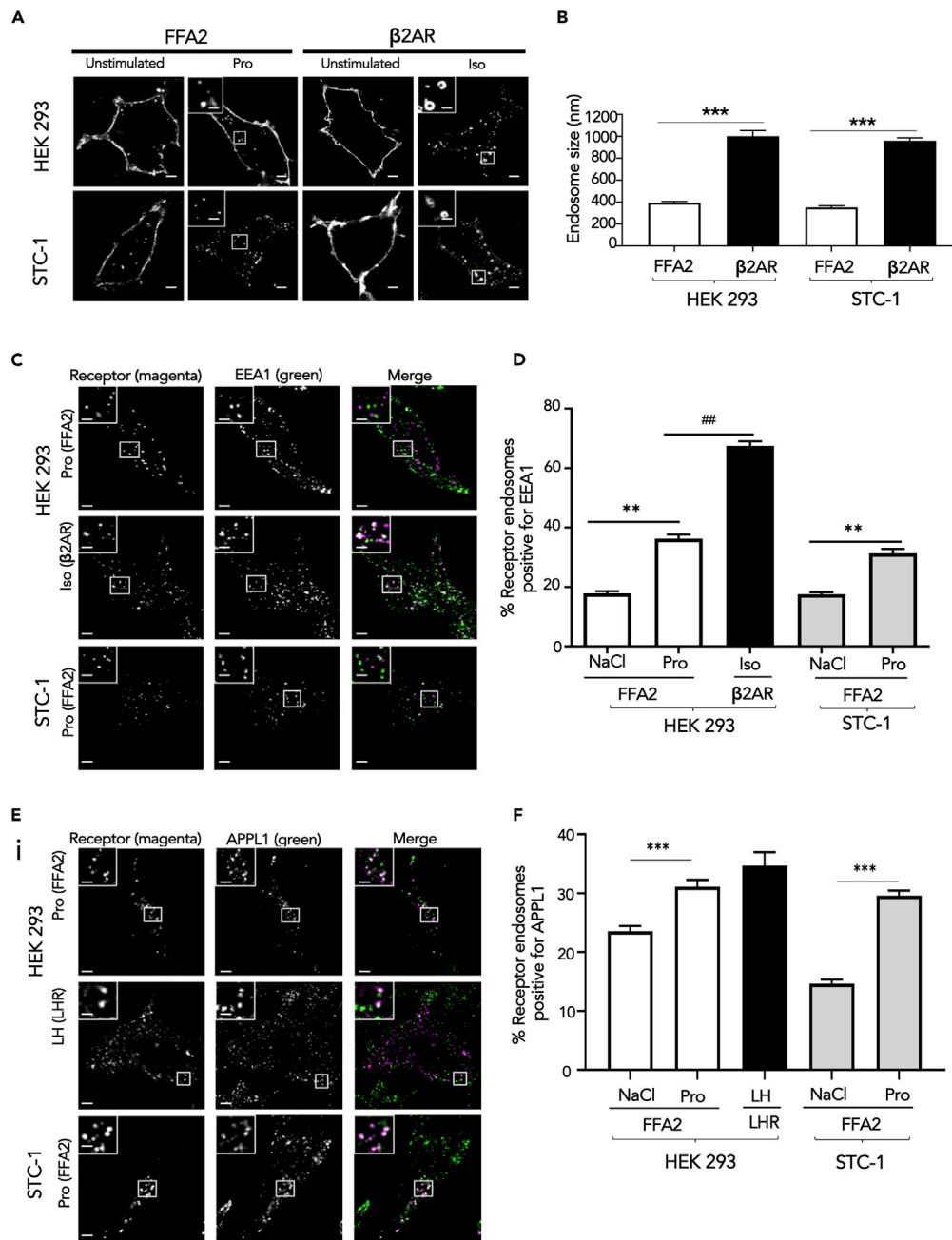


**Figure 3. FFA2 Internalizes to Endosomes Exhibiting Properties of VEEs**

(A) Representative confocal microscopy images of HEK 293 cells expressing FLAG-FFA2 or FLAG-β2AR or STC-1 cells expressing FLAG-FFA2 or FLAG-β2AR imaged live with confocal microscopy before and after ligand treatment. FFA2 was stimulated with sodium propionate (Pro) (1 mM), and β2AR with isoproterenol (Iso, 10 μM) for 20 min. Scale bars, 5 μm; scale bar in inset, 1 μm.

(B) Bar graph showing diameter of FFA2 or β2AR in HEK 293 or STC-1 cells containing endosomes. Endosome diameter was assessed by measuring the diameter of 20 endosomes, n = 10 cells per condition, collected across three independent experiments. Two-sided Mann-Whitney U test, \*\*\*p < 0.001.

(C) Representative confocal microscopy images of fixed HEK 293 cells stably expressing FLAG-FFA2 or β2AR or STC-1 cells transiently expressing FLAG-FFA2 treated with ligand for 20 min prior to “stripping” by PBS/EDTA (to remove surface bound FLAG antibody), fixation and stained with anti-EEA1 antibody. Scale bars, 5 μm; scale bar in inset, 1 μm.

(D) Numbers of FFA2 or β2AR-containing endosomes positive for EEA1 quantified from (C); 200 endosomes per condition, 10 cells quantified per condition. Data represent mean ± SEM, n = 10 cells per condition, collected across

**Figure 3. Continued**

three independent experiments. Two-sided Mann-Whitney U test, \*\* $p < 0.01$ , ### $p < 0.01$ . (E, F) FFA2 colocalizes with APPL1.

(E) Representative confocal microscopy images of fixed HEK 293 cells stably expressing FLAG-FFA2 or LHR or STC-1 cells transiently expressing FLAG-FFA2 treated with ligand (LH for LHR). Cells were treated as in (C) except that cells were stained with anti-APPL1 antibody. Scale bars, 5  $\mu\text{m}$ ; scale bar in inset, 1  $\mu\text{m}$ .

(F) Numbers of FFA2 or LHR-containing endosomes positive for APPL1 quantified from (E); 200 endosomes per condition, 10 cells quantified per condition.  $n = 10$  cells per condition, collected across three independent experiments. Two-sided Mann-Whitney U test, \*\*\* $p < 0.001$ . For confocal images, representative images are shown of  $\sim 10$  cells/experiment. Data represent mean  $\pm$  SEM.

See also [Figure S6](#).

activation of  $G\alpha i/o$  signaling ([Figure 2H](#)). Overall, these data demonstrate a requirement for ligand-induced FFA2 internalization in propionate-mediated  $G\alpha i/o$  signaling in heterologous and enteroendocrine cells.

**FFA2 Internalizes to Very Early Endosomes for Sorting and Signaling**

We have previously shown that GPCRs exhibit divergent sorting to distinct endosomal compartments between early endosomes (EEs) and very early endosomes (VEEs), and this post-endocytic organization is critical for both GPCR sorting fate and endosomal signaling ([Jean-Alphonse et al., 2014](#); [Sposini et al., 2017](#)). As internalization of FFA2 is essential for its  $G\alpha i/o$  signaling, we next determined the postendocytic compartment that FFA2 internalizes to. The organization of FFA2 across VEEs and EEs was compared with the  $\beta 2$ -adrenergic receptor ( $\beta 2\text{AR}$ ), a GPCR known to be rapidly sorted to the EE compartment ([Jean-Alphonse et al., 2014](#)). VEEs are one-third the diameter of EEs and lack classic EE markers such as early endosomal autoantigen 1 (EEA1); however, a subpopulation of VEEs contains the adaption protein APPL1 (adaptor protein phosphotyrosine interaction, pleckstrin homology domain, and leucine zipper containing 1), which plays essential roles in driving recycling from the VEE and in negative regulation of G protein signaling from this compartment ([Jean-Alphonse et al., 2014](#); [Sposini et al., 2017](#)).

Internalization of FLAG-FFA2 was imaged in both live HEK 293 and STC-1 cells over time (0–30 min). FFA2 internalized to endosomes  $\sim 400$  nm diameter within 5 min of ligand stimulation ([Figures 3A, 3B, and S6](#)), in contrast to the significantly larger size of endosomes containing internalized  $\beta 2\text{AR}$  ([Jean-Alphonse et al., 2014](#)) ([Figure 3A](#)). Furthermore, the majority ( $>60\%$ ) of constitutive and ligand-induced internalized FFA2 did not traffic to an EEA1-positive EE compartment, compared with  $\sim 70\%$  for  $\beta 2\text{AR}$  that did localize to EEA1-positive endosomes ([Figures 3C and 3D](#)), suggesting that FFA2 may traffic primarily to VEEs than EEs. This was further supported by the finding that a subpopulation of internalized FFA2 co-localizes with APPL1 ( $32.8 \pm 0.35\%$  following propionate treatment), similar to that observed with the luteinizing hormone receptor (LHR;  $35.2 \pm 1.92\%$ ), a GPCR known to traffic to VEEs ([Sposini et al., 2017](#)) ([Figures 3E and 3F](#)).

As FFA2 was primarily targeted to the VEE and propionate-induced FFA2 signaling requires internalization in enteroendocrine cells, we next investigated whether this compartment regulates FFA2 activity. We previously demonstrated that APPL1 is essential in rapid recycling of GPCRs targeted to this compartment back to the plasma membrane ([Sposini et al., 2017](#)). To determine a functional requirement of APPL1 on FFA2 trafficking, cellular levels of APPL1 were depleted via small interfering RNA (siRNA) in HEK 293 cells stably expressing FLAG-FFA2 ([Figure 4A](#)). We first examined the post-endocytic fate of FLAG-FFA2 when activated by propionate by confocal microscopy. APPL1 knockdown strongly impaired propionate-induced FFA2 recycling; in contrast, there was no effect in cells treated with NaCl (constitutive trafficking) as there was a complete return of the receptor back to the plasma membrane within 1 h following removal of ligand ([Figure 4B](#)). The role of APPL1 in rapid FFA2 recycling was quantitated via live-cell total internal reflection fluorescence microscopy (TIRFM) of an FFA2 tagged at the extracellular N terminus with pH-sensitive GFP super-ecliptic pHluorin (SEP). SEP fluoresces in an extracellular neutral pH environment but is non-fluorescent when confined to the acidic lumen of endosomes and therefore enables the detection of receptors upon insertion into the plasma membrane ([Miesenbock et al., 1998](#); [Yudowski et al., 2007](#)). TIRFM imaging of SEP-tagged FFA2 (SEP-FFA2) established that FFA2 recycling events (identified as “puffs” of GFP fluorescence at the membrane [[Figure S7A](#)]) were transient and increased significantly within 5 min of propionate treatment, whereas treatment with NaCl exhibited a low rate of basal events ([Figures S7B, S7C, and 4B](#)), suggesting constitutively internalized FFA2 is sorted to a distinct slow recycling pathway. The



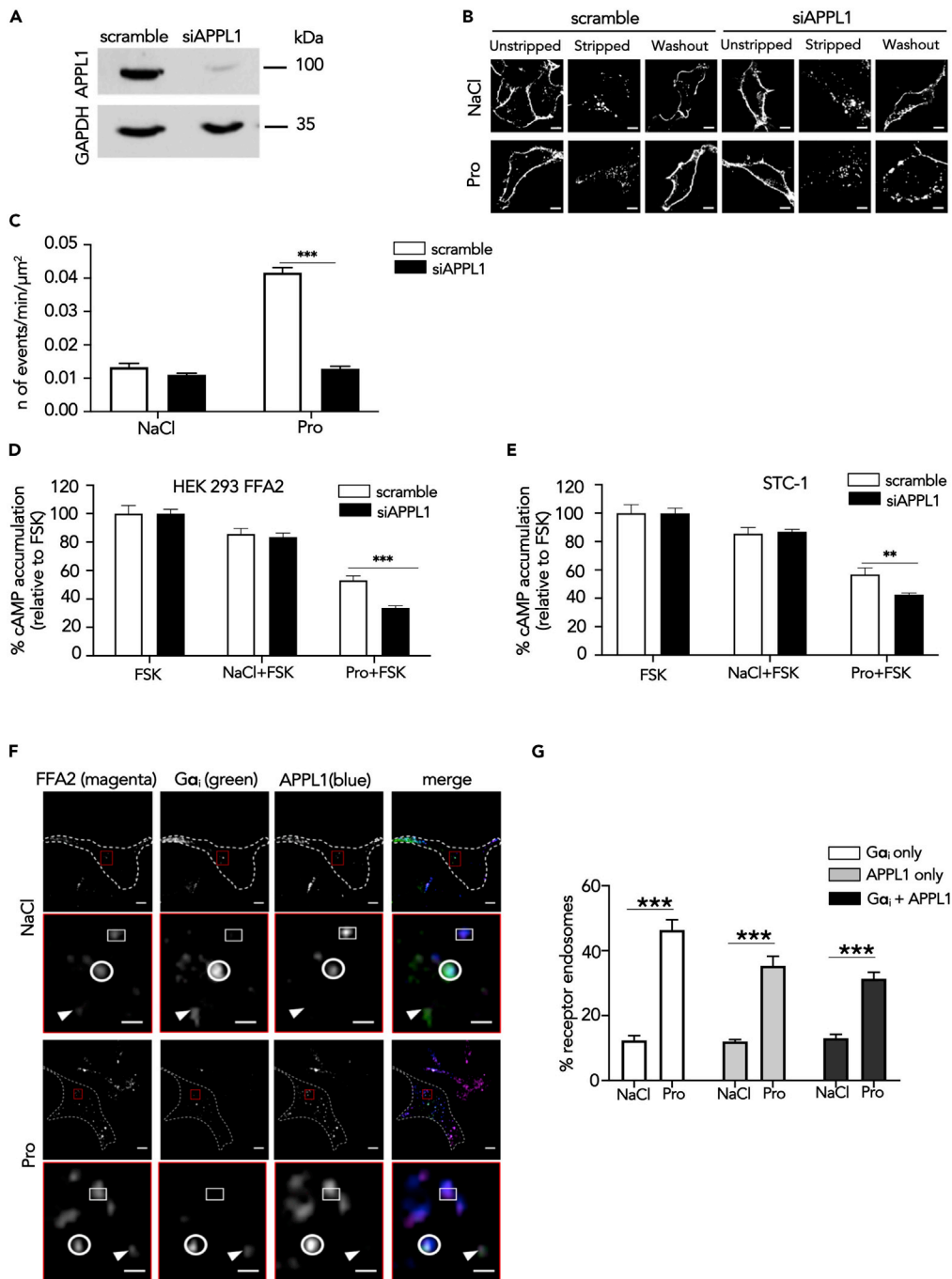


**Figure 4. FFA2 Trafficking and G Protein Signaling Is Regulated by APPL1**

(A) Representative western blot of total cellular levels of APPL1 from cells transfected with either scramble or APPL1 siRNA. GAPDH was used as a loading control.

(B) Representative confocal microscopy images of propionate-induced internalization and recycling following APPL1 siRNA-mediated knockdown. HEK 293 cells stably expressing FLAG-FFA2 were labeled with anti-FLAG antibody and then treated with NaCl (1 mM) or propionate (Pro) (1 mM) for 20 min, then “stripped” and incubated with ligand-free medium for 1 h to allow receptor recycling. Scale bars, 5  $\mu\text{m}$ .

(C) Recycling of HEK 293 cells stably expressing SEP-FFA2 was measured in real time, via TIRFM; cells were transfected either with scramble or APPL1 siRNA and stimulated with NaCl (1 mM) or sodium propionate (Pro) (1 mM) for 5 min  $n = 20$  cells per condition, collected across four independent experiments. Two-sided Mann-Whitney U test, \*\*\* $p < 0.001$ .

**Figure 4. Continued**

(D and E) APPL1 negatively regulates propionate-mediated  $G\alpha_i$  signaling. HEK 293 cells stably expressing FLAG-FFA2 (D) or STC-1 cells (E) transfected with either scramble of APPL1 siRNA prior to pre-treatment of IBMX (0.5 mM, 5 min) and then stimulated with forskolin (FSK, 3  $\mu$ M) or a combination of FSK and NaCl or stated SCFAs (1 mM, 5 min). Data are expressed as percent change of FSK and NaCl treatment.  $n = 4$  independent experiments. Two-sided Mann-Whitney U test, \* $p < 0.05$ ; \*\* $p < 0.01$ .

(F and G) FFA2 colocalizes with  $G\alpha_i$  within APPL1 endosomes. Representative TIRFM images of HEK 293 cells stably expressing FLAG-FFA2 (magenta),  $G\alpha_i$  (green), APPL1 (blue) in cells stimulated either with NaCl (1 mM) or sodium propionate (Pro) (1 mM) for 5 min (F). Dotted line marks cell boundary. The lower panel of each treatment, highlighted in red, shows higher magnification image of the region of colocalization indicated by the red box in the corresponding upper-panel image. Arrows indicate FFA2 endosomes positive for  $G\alpha_i$  only; circle indicates FFA2 endosomes positive for  $G\alpha_i$  and APPL1; squares indicate FFA2 endosome positive for APPL1 only. Scale bars of upper-panel images, 10  $\mu$ m; scale bar of lower-panel images 1  $\mu$ m. (G) Quantification of FFA2 endosomes positive for  $G\alpha_i$ , APPL1, or  $G\alpha_i$  and APPL1;  $n = 12$  cells per condition from (F) were quantified across three independent experiments. Two-way ANOVA, Bonferroni multiple comparisons test, \*\*\* $p < 0.001$ . Data represent mean  $\pm$  SEM.

See also [Figures S7](#) and [S8](#).

frequency of these events remained constant throughout the duration of the imaging period (30 min) ([Figure S7C](#)). These plasma membrane insertion events were not affected by pre-treatment of cells with cycloheximide, suggesting that such events are not due to *de novo* receptor biogenesis ([Figure S7D](#)). In cells depleted of APPL1, however, propionate-induced, but not constitutive, recycling of SEP-FFA2 was significantly impaired ([Figure 4C](#)).

In addition to regulating the post-endocytic sorting of VEE targeted receptors, APPL1 also negatively regulates GPCR/ $G\alpha_s$  signaling from this compartment ([Sposini et al., 2017](#)). As we have demonstrated that propionate-induced  $G\alpha_i/o$  signaling requires receptor internalization, we next examined the potential role of the VEE in FFA2 signaling. Depletion of APPL1 resulted in a 2-fold increase in propionate-mediated inhibition of forskolin-stimulated cAMP ([Figure 4D](#)), suggesting that APPL1 can also negatively regulate heterotrimeric  $G\alpha_i/o$  signaling in addition to  $G\alpha_s$  signaling. Negative regulation of  $G\alpha_i/o$  signaling by APPL1 was conserved in STC-1 cells as depletion of APPL1 levels also resulted in a significant enhancement of propionate-mediated inhibition of forskolin-induced cAMP ([Figures S8](#) and [4E](#)).

The above data suggest that propionate-induced  $G\alpha_i/o$  signaling may occur from VEEs, and be regulated by APPL1 endosomes; therefore, we next determined whether FFA2 colocalizes with  $G\alpha_i$  in APPL1-positive endosomes to determine if this G protein machinery is present in this compartment. HEK 293 cells expressing FLAG-FFA2 and  $G\alpha_i$ -Venus were imaged via TIRFM as VEEs are prevalent in the peripheral juxtamembrane region of cells ([Sposini et al., 2017](#)). TIRFM analysis revealed that FFA2 and  $G\alpha_i$ -Venus-positive endosomes are heterogeneous and characterized by FFA2- $G\alpha_i$  endosomes with and without APPL1. In addition, FFA2 endosomes were also positive for APPL1 where no  $G\alpha_i$  was present ([Figures 4F](#) and [4G](#)). Overall, these data demonstrate that APPL1 is essential for propionate-induced FFA2 trafficking and regulation of propionate-mediated  $G\alpha_i/o$  signaling.

**Propionate-Induced GLP-1 Release Requires Receptor Internalization and  $G\alpha_i/o$  Signaling**

As propionate-induced  $G\alpha_i/o$  signaling requires FFA2 internalization, we next assessed whether such a pathway regulates GLP-1 secretion. First, we examined the involvement of  $G\alpha_i/o$  versus  $G\alpha_q/11$  signaling in mediating propionate-induced GLP-1 release, using  $G\alpha_i/o$  or  $G\alpha_q/11$  inhibitors at concentrations that we demonstrated could inhibit receptor signaling in enteroendocrine cells ([Figures 1A](#), [1B](#), and [S3](#)). STC-1 cells or colonic crypts pretreated with Ptx impaired propionate-induced GLP-1 release ([Figures 5A](#) and [5B](#)). In contrast, pretreatment of STC-1 cells with the  $G\alpha_q/11$  inhibitor, YM-254890, had no significant effect on propionate-mediated GLP-1 release ([Figure 5C](#)). In colonic crypts, propionate-induced GLP-1 release in the presence of YM-25480 was impaired when assessing the ability of propionate to induce hormone release over NaCl treatment ([Figure 5Di](#)), although fold change responses were not significantly different between crypts treated with or without YM-254890 ([Figure 5Dii](#)). As we did not observe propionate-induced  $G\alpha_q/11$  signaling in colonic crypts ([Figures 1F–1I](#)), we determined if propionate-mediated FFA2  $G\alpha_i/o$  signaling is altered in the presence of YM-25480 in these primary cultures. In the presence of YM-25480, propionate-mediated inhibition of forskolin-induced cAMP was partially, but significantly, impaired compared with control treated cells ([Figure S9A](#)). This was only specific to propionate-mediated FFA2 signaling, as YM-25480 had no effect on propionate-mediated signaling from FFA3, a receptor

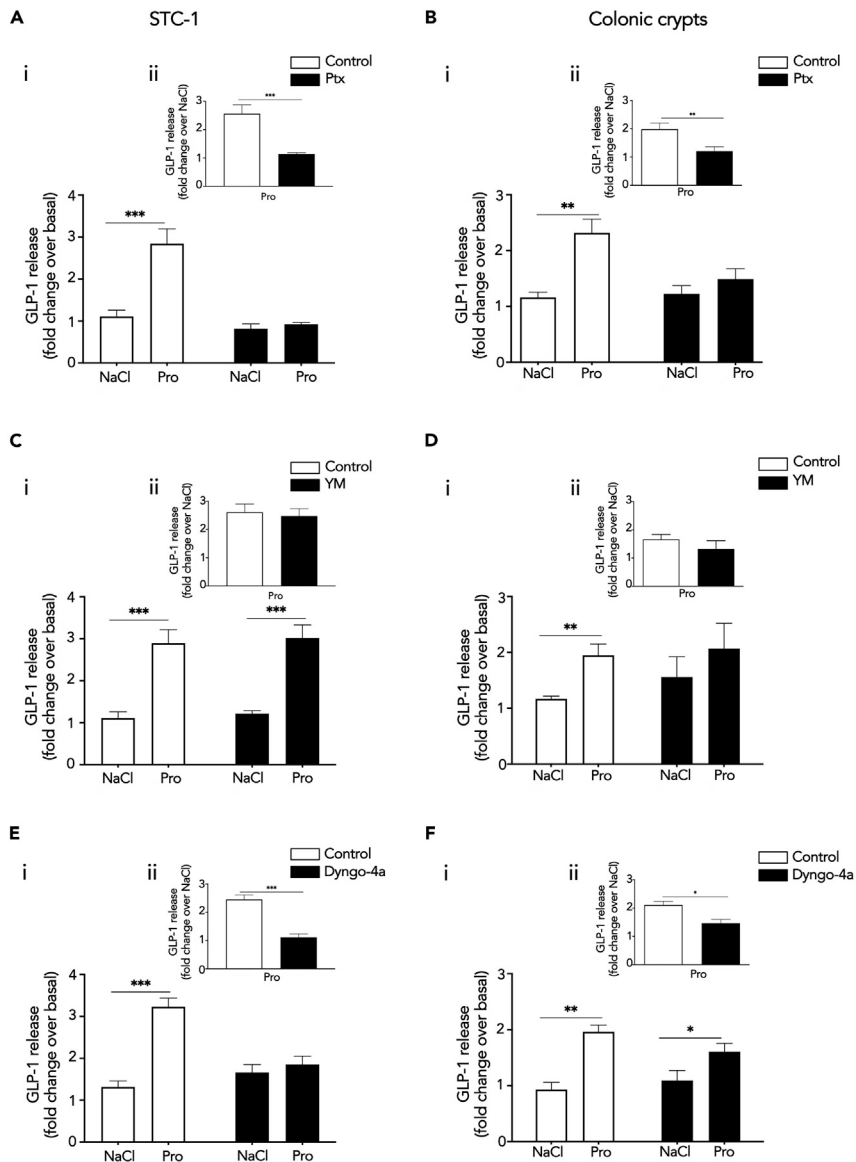


**Figure 5. Endosomal *Gxi/o* Signaling Regulates Propionate-Mediated GLP-1 Release**

Stimulation of GLP-1 release from STC-1 cells (A) or colonic crypts (B) in the presence of Ptx. STC-1 cells or colonic crypts were pre-treated with either vehicle or Ptx (200 ng/mL, 20 h) prior to stimulation with either NaCl (1 mM) or sodium propionate (Pro) (1 mM) for 2 and 1 h for colonic crypts. For STC-1 cells,  $n = 4$  independent experiments. For crypts,  $n = 8$  independent experiments. Two-sided Mann-Whitney U test,  $***p < 0.001$ . Stimulation of GLP-1 release from STC-1 cells (C) or colonic crypts (D) in the presence of *Gxi*/11 inhibitor, YM-254890. STC-1 cells and colonic crypts were pre-treated with either DMSO or YM-254890 (YM, 10  $\mu$ M, 5 min) and then treated as in (A) and (B). For STC-1 cells,  $n = 4$  independent experiments. For crypts,  $n = 3$  independent experiments. Two-sided Mann-Whitney U test,  $*p < 0.05$ ,  $**p < 0.01$ . Stimulation of GLP-1 release from STC-1 cells (E) or colonic crypts (F) in the presence of Dyngo-4a. STC-1 cells or colonic crypts were pre-treated with either DMSO or Dyngo-4a (50  $\mu$ M, 45 min for STC-1 cells and 100  $\mu$ M, 45 min for colonic crypts), following pre-treatment, Dyngo-4a was co-incubated with ligands for an additional 5 min and then removed. Cells and crypts were treated as in (A) and (B). For STC-1 cells,  $n = 5$  independent experiments. For crypts,  $n = 3$  independent experiments. Two-sided Mann-Whitney U test,  $**p < 0.01$ ,  $***p < 0.001$ . Insets show propionate-induced GLP-1 release normalized to NaCl GLP-1 release.  $**p < 0.01$ ,  $***p < 0.001$ . GLP-1 secretion of media and cells was detected via RIA and was expressed as fold change of total GLP-1 and normalized to NaCl secretion within the same experiment. Data represent mean  $\pm$  SEM. See also [Figures S9](#) and [S10](#).

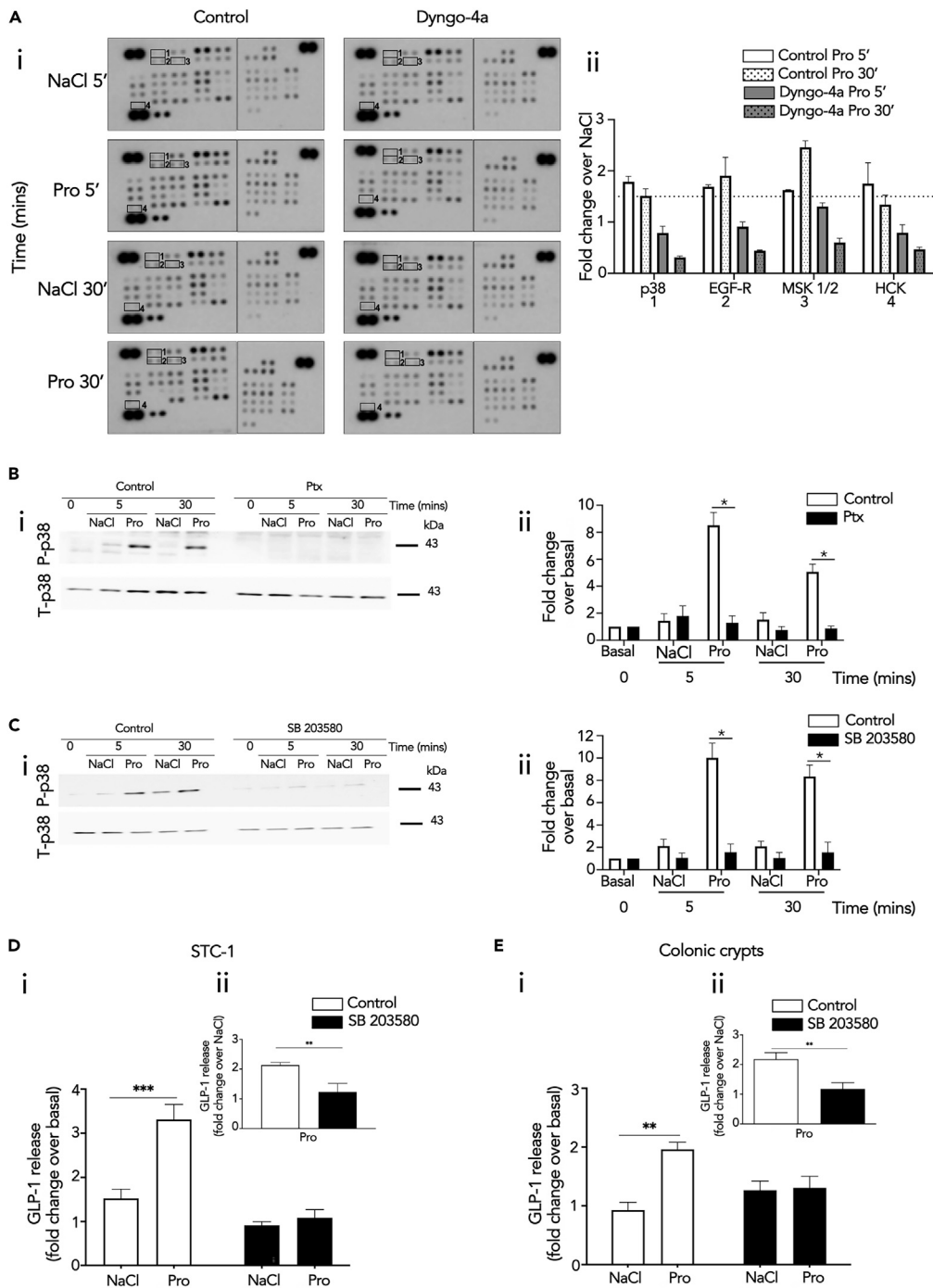


**Figure 6. Endosomal Signaling of FFA2 Regulates GLP-1 Release via Activation of p38**

(A) STC-1 cells were pre-treated with DMSO (vehicle) or Dyngo-4a (50  $\mu$ M, 45 min) prior to stimulation with NaCl (1 mM) or propionate (Pro) (1 mM) for 5 or 30 min. Lysates were incubated with membranes spotted for 43 different phosphokinases (R&D systems). (Ai) Membranes highlighting location of phospho-kinase antibodies spotted onto the array. Signals of relevant kinases effected by Dyngo-4a are indicated by numbers. (Aii) Fold changes over NaCl in levels of phosphorylation that decreased in presence of Dyngo-4a. Data represent mean  $\pm$  SEM of fold change values. (B–E) Representative western blots demonstrating phosphorylated p38 (P-p38) and total p38 (T-p38) of lysates from STC-1 cells pre-treated with either Ptx (B) or p38 inhibitor, SB 203580 (C). STC-1 cells were pre-treated with control or Ptx (200 ng/mL, 20 h) or SB 203580 (5  $\mu$ M, 10 min) prior to stimulation of NaCl (1 mM) or propionate (Pro) (1 mM) at the

**Figure 6. Continued**

indicated time points. Cell lysates were then collected for western blot analysis and probed for P-p38. Membranes were then stripped and re-probed with T-p38, which was used as a loading control (i). Densitometry and fold change analysis of P-p38 normalized to T-p38 of lysates pre-treated with Ptx, or SB 203580. Fold change of densitometry analysis of P-p38 levels normalized to basal of control or inhibitor at each time point stimulation with T-p38 (ii). Stimulation of GLP-1 release from STC-1 cells (D) or colonic crypts (E) in the presence of SB 203580. Both were pre-treated either with DMSO or SB 203580 (5  $\mu$ M, 10 min), prior to stimulation with either NaCl (1 mM) or sodium propionate (Pro) (1 mM) for 2 h for STC-1 cells and 1 h for colonic crypts. For STC-1 cells and crypts, n = 3 independent experiments. Two-sided Mann-Whitney U test, \*\*\*p < 0.001. Insets show propionate-induced GLP-1 release normalized to NaCl-induced GLP-1 release. \*\*p < 0.01, \*\*\*p < 0.001. GLP-1 secretion of media and cells detected via RIA and was expressed as fold change of total GLP-1 and normalized to NaCl secretion within the same experiment. Data represent mean  $\pm$  SEM.

coupled to *Gai/o* and not *G $\alpha$ q/11* (Figure S9B). Together, these data suggest that, in STC-1 cells and colonic crypts, propionate induces GLP-1 secretion via a *Gai/o*-dependent mechanism.

The requirement of *Gai/o* signaling for propionate-mediated GLP-1 release, and the critical role of propionate-driven FFA2 internalization for G protein signaling, suggests a role for propionate-induced receptor internalization. To test this hypothesis, receptor endocytosis in STC-1 cells was blocked by Dyngo-4a treatment (Figure 2G). In cells treated with Dyngo-4a, propionate exhibited a marked reduction in GLP-1 release compared with control treated cells (Figure 5E). This inhibition by Dyngo-4a was not a result of an overall decreased capacity for these cells to secrete hormone as forskolin-induced GLP-1 release was not affected by inhibition of dynamin GTPase activity (Figure S10A). In colonic crypts, pretreatment with Dyngo-4a, impaired propionate-induced GLP-1 release but not to the same degree as observed in STC-1 cells (Figure 5F). As we have observed a dependence of propionate-driven FFA2 internalization for not only G protein signaling in STC-1 cells (Figure 2H) but also for GLP-1 release, we hypothesized that the differences in the inhibition of propionate-induced GLP-1 release by Dyngo-4a in colonic crypts may be due to more technical limitations of Dyngo-4a in primary crypts compared with a monolayer of cells. To assess this, we determined the ability of propionate to inhibit forskolin-induced cAMP in the presence of Dyngo-4a in colonic crypts. In the presence of Dyngo-4a, propionate-mediated inhibition of forskolin-induced cAMP was significantly, but only partially, impaired compared with control treated cells (Figure S10B), in contrast to the full inhibition of *Gai/o* signaling by Dyngo-4a observed in STC-1 cells (Figure 2H). Thus, the level of propionate-dependent *Gai/o* signal inhibition by Dyngo-4a correlates with its ability to inhibit propionate-driven gut hormone secretion. Overall, this suggests that internalization-dependent *Gai/o* signaling mediates propionate-induced GLP-1 release.

**Internalization-Dependent Propionate Signaling Regulates GLP-1 Release via Activation of p38**

Increases in intracellular cAMP is an established driver of gut hormone release, yet our data indicates propionate induces gut hormone release in a *Gai/o*-dependent manner, a pathway that decreases cAMP levels. Therefore, we hypothesized that the mechanism mediating endosomal *Gai/o*-dependent GLP-1 release is potentially via distinct downstream pathways activated by *Gai/o*, rather than its actions on its effector enzyme adenylate cyclase. Thus, we determined which propionate-mediated signaling pathways downstream of G protein signaling are also spatially regulated. A phosphokinase array was employed in STC-1 cells to identify propionate-induced signaling pathways dependent on receptor internalization. STC-1 cells were pretreated with Dyngo-4a and stimulated with propionate for 5 or 30 min. The array revealed that 16 of the 43 kinases within the array were phosphorylated after 5 or 30 min of propionate treatment. However, only p38 $\alpha$ , EGF-R, MSK1/2, and Hck showed reduced phosphorylation when internalization was inhibited (Figure 6A). Of these kinases, p38 $\alpha$  was selected for further analysis as this kinase and MSK1/2 are part of the same signal cascade. Furthermore, p38 $\alpha$  is known to be activated at endosomes by other GPCRs (Grimsey et al., 2015). We then asked if propionate-induced p38 activation was *Gai/o*-mediated. To test this, propionate-induced p38 activation was assessed in STC-1 pretreated with Ptx via western blot. Pretreatment of Ptx significantly impaired propionate-induced p38 signaling (Figure 6B).

Since propionate-induced activation of p38 involves receptor internalization and *Gai/o* signaling, its role in propionate-induced GLP-1 release was assessed. A widely used selective p38 inhibitor SB 203580, which inhibits the catalytic activity of p38- $\alpha$  and - $\beta$  isoforms without inhibiting p38 phosphorylation mediated by upstream kinases (Ge et al., 2002), was employed and significantly impaired propionate-induced

activation of p38 (Figure 6C). In STC-1 cells and colonic crypts, SB 203580 pretreatment significantly impaired propionate's ability to induce GLP-1 secretion (Figures 6D and 6E) suggesting that propionate-induced  $G\alpha i$  signaling regulates GLP-1 release via a p38-dependent mechanism.

## DISCUSSION

The ability of propionate to stimulate the release of anorectic gut hormones via the GPCR FFA2 represents a key physiological function of high interest owing to its demonstrated health benefits (Chambers et al., 2015, 2019). However, despite our increasing knowledge of the complexity of GPCR signaling networks in other cell systems, the underlying mechanisms regulating gut hormone release by propionate/FFA2 are poorly understood. In this study we demonstrate that signaling and downstream functions of FFA2, in response to propionate, are specified through tight control of receptor location.

In the gut, the current view is that GPCRs coupled to either  $G\alpha s$ -cAMP or  $G\alpha q/11$ - calcium pathways mediate anorectic gut hormone release (Hauge et al., 2017; Tian and Jin, 2016). From a receptor perspective, however, it is well known that many GPCRs are pleiotropically coupled, either directly or via receptor cross talk, and where additional mechanisms, such as intracellular receptor signaling, enable diversity in cell functions from the same G protein and second messenger system. Furthermore, different GPCR ligands (endogenous and synthetic) can elicit distinct conformational states and thus the potential to induce bias signal activity from the same receptor. In regard to FFA2 activity, which has been characterized previously as a dually coupled GPCR in studies primarily in heterologous cells (Brown et al., 2003; Le Poul et al., 2003), to date there have been no studies demonstrating its pleiotropic coupling to both  $G\alpha i/o$  and  $G\alpha q/11$  in the gut at the level of second messenger signaling. Thus, to delineate the mechanisms of propionate-induced GLP-1 release from enteroendocrine cells, we first profiled the second messenger signaling activated by this SCFA in our intestinal models. Although propionate robustly signals via  $G\alpha i/o$  in a FFA2-dependent manner, it was unable to induce  $G\alpha q/11$  signaling both in colonic crypts and STC-1 cells. This is in contrast to prior studies reporting a propionate-dependent calcium response in colonic cultures expressing Venus fluorescent protein in enteroendocrine L cells (Tolhurst et al., 2012). The reasons for this disparity are unclear but could relate to either the mouse model harboring Venus protein, longer culture times employed to create dispersed colonic cultures to measure calcium signaling, as opposed to the intact colonic crypts used in this study, and/or reflect a  $G\alpha i/o$ -mediated response as  $G\alpha i/o$ -coupled GPCRs are known to modulate calcium responses, including influx of extracellular calcium (Tang et al., 2015; Alkhatib et al., 1997). To our knowledge this is also the first demonstration that previously characterized synthetic orthosteric and allosteric FFA2 selective ligands activate  $G\alpha q/11$  signaling in the colon. Although propionate may also activate FFA3, a  $G\alpha i/o$ -coupled receptor known to also be expressed in the colon, it was demonstrated in this study that colonic crypts from FFA2 KO animals are unable to activate SCFA-dependent  $G\alpha i/o$  signaling and that these animals do not exhibit altered FFA3 levels. This supports prior published work from us and others demonstrating SCFA-mediated GLP-1 release requires FFA2 (Tolhurst et al., 2012; Psichas et al., 2015). FFA2 is known to be a dually coupled receptor in HEK 293 or CHO cells (Le Poul et al., 2003), and indeed our data in HEK 293 cells expressing FFA2 are consistent with these reports, whereby propionate also activates  $G\alpha q/11$  signaling. This potential system-dependent bias exhibited by FFA2 and propionate is intriguing given FFA2 can activate  $G\alpha q/11$  signaling in enteroendocrine cells when stimulated with synthetic ligands. One potential mechanism for the distinct propionate/FFA2 signal profiles between enteroendocrine cells and heterologous cells is cross talk of FFA2 with another GPCR such as FFA3. However, it has recently been demonstrated that FFA2- $G\alpha q/11$  signaling is not decreased, but enhanced, via associations with FFA3 (Ang et al., 2018).

Propionate's inability to induce  $G\alpha q/11$ -mediated intracellular calcium mobilization is indeed paradoxical to what is known about the signaling requirements of anorectic gut hormone secretion (Spreckley and Murphy, 2015). Although we do not detect propionate-induced  $G\alpha q/11$  signaling from FFA2, this does not exclude a role for calcium, from intracellular or extracellular sources, overall in downstream steps of GLP-1 secretion and modulation of the exocytic machinery. However, exocytosis is known to occur via either calcium-dependent or -independent pathways (Sato et al., 1998; Komatsu et al., 1995) and also involving  $G\alpha i$  (Aridor et al., 1993; Kreft et al., 1999; Mansvelter et al., 2002), including an ability for the  $G\alpha i$ -coupled FFA3 to induce GLP-1 release when stimulated with a FFA3-selective ligand (Nøhr et al., 2013). Although we observed that propionate-induced GLP-1 release was impaired in the presence of Ptx in STC-1 cells and colonic crypts, this is inconsistent with previous reports that did not find propionate-induced GLP-1 release to be modulated by Ptx (Tolhurst et al., 2012; Bolognini et al., 2016) but is



impaired by the  $G\alpha q/11$  inhibitor, FR900359 (Bolognini et al., 2016). However, confirmation of Ptx-dependent inhibition of propionate-mediated  $G\alpha i/o$  signaling at the second messenger level in STC-1 cells or crypts was not reported in these prior studies. Although FR900359 has been shown to also inhibit  $G\beta\gamma$ -mediated signaling from  $G\alpha i/o$ -coupled receptors (Gao and Jacobson, 2016), we observed that inhibition of  $G\alpha q/11$  activation partially inhibited propionate-FFA2  $G\alpha i/o$  signaling but not FFA3  $G\alpha i/o$  signaling, suggesting that an active  $G\alpha q/11$  is integrated with FFA2  $G\alpha i/o$  signaling. Such cross talk may be analogous to the findings that arrestin-mediated signaling of GPCRs requires an active G protein conformational state perhaps even in the absence of second messenger responses (Grundmann et al., 2018).

Our results demonstrating propionate-mediated GLP-1 release via  $G\alpha i/o$  suggest that mechanisms regulating propionate-induced release of GLP-1 may be more complex and not via  $G\alpha i/o$ -mediated decreases in cAMP levels per se, a second messenger that induces gut hormone release (Hauge et al., 2017). One mechanism that can diversify downstream cellular functions from a common upstream pathway is via spatial control of signaling. Indeed, agonist induced FFA2 internalization differentially regulated  $G\alpha i$  and  $G\alpha q/11$  signaling, indicating at least in HEK 293 cells that FFA2/ $G\alpha i$  signaling was from internalized receptor and  $G\alpha q/11$  signaling occurred from the plasma membrane. Spatial discrimination in GPCR/G protein signaling has been observed with the pleiotropically coupled calcium-sensing receptor (Gorvin et al., 2018). The specific requirement for receptor internalization in driving FFA2-mediated  $G\alpha i/o$  signaling was conserved in enteroendocrine cells, whereby this pathway mediated GLP-1 release, providing a novel mechanism underlying propionate's downstream functions in the gut. We also identified that FFA2 primarily traffics to the VEE in HEK 293 and STC-1 cells, an endosomal compartment we have previously shown to be critical for sorting and endosomal signaling for a subset of GPCRs (Jean-Alphonse et al., 2014; Sposini et al., 2017). For GPCRs that are trafficked to the small endosomes of the VEE, APPL1 has been demonstrated to be crucial for both receptor recycling and negative regulation of  $G\alpha s$  signaling. We demonstrate that rapid ligand-induced recycling of FFA2 is also APPL1 dependent and negatively regulates FFA2-endosomal  $G\alpha i/o$  signaling in HEK 293 and enteroendocrine cells, indicating that the APPL1/VEE compartment can negatively regulate distinct G protein pathways, in addition to  $G\alpha s$ -coupled GPCRs (Sposini et al., 2017).

Given the requirement for receptor internalization in  $G\alpha i/o$  signaling and propionate-induced gut hormone release, we hypothesized that additional  $G\alpha i/o$ -activated pathways were important in gut hormone secretion. We identified that phosphorylation of a small subset of downstream kinases required FFA2 internalization when activated by propionate, which suggests a potential role for endomembrane signaling in providing a signal platform to activate unique signaling substrates from the plasma membrane, or indeed other intracellular compartments (Eichel and Von Zastrow, 2018; Hanyaloglu, 2018). We focused on p38 as kinases of the same pathway, MSK1/2, were also identified in the array, and p38 is known to be activated at endosomes by other GPCRs (Grimsey et al., 2015). Propionate has also previously been shown to activate p38 in many cellular systems and has a role in regulating inflammatory responses (Rutting et al., 2019; Yonezawa et al., 2007; Ang et al., 2018). For enteroendocrine cells and colonic crypts, we identify a key role of p38 in regulating propionate-induced GLP-1 release. Interestingly, p38 is also involved in regulating GLP-1 secretion induced by meat hydrolysate and essential amino acid and low-molecular-weight chitosan (Reimer, 2006; Liu et al., 2013). More recently, propionate-induced GLP-1 release was also found to be regulated by p38 in chicken intestinal epithelial cells (Zhang et al., 2019), suggesting a conserved role of this kinase in anorectic gut hormone secretion induced by distinct metabolites. How p38 may regulate gut hormone secretion is unknown, although this kinase pathway may phosphorylate components of the SNARE complex such as syntaxin1a, shown recently to be essential for GLP-1 secretion in intestinal L-cells (Wheeler et al., 2017; Campbell et al., 2020).

Together, these findings support a model whereby propionate regulates anorectic gut hormone secretion by a tightly controlled mechanism involving integration of membrane trafficking and intracellular signaling. As more GPCRs are shown to traffic and be spatially regulated by this and other intracellular compartments, our studies may form the basis for a broader mechanism employed by intestinal metabolites, which activate multiple GPCRs within the gut, to diversify its functions *in vivo*.

### Limitations of the Study

This study demonstrates that the tight integral regulation of membrane trafficking and intracellular signaling is critical for propionate-induced secretion of anorectic gut hormone. However, a limitation of the current study is that it does not directly demonstrate that FFA2 signaling from the VEE specifically

mediates gut hormone release. In addition to APPL1, other proteins that occupy the VEE are unknown. Furthermore, APPL1, although essential for regulating recycling and acute G protein signaling of GPCRs specifically targeted to the VEE, is also found in other compartments. Future studies will be directed to identify the proteins that comprise the VEE compartment and could be exploited to directly image and assess the role of signaling from this compartment in the intestine, and indeed other tissues where FFA2 is expressed. An additional consideration is that, although FFA2 trafficking is regulated in STC-1 cells, they are not polarized cells as in the intestinal crypt. Thus, post-endocytic organization of receptors across the VEE and other membrane trafficking compartments at the apical and basal side may represent an additional level of spatial organization.

### Resource Availability

#### Lead Contact

Further information and request for resources should be directed to and will be fulfilled by the Lead Contact, Aylin Hanyaloglu ([a.hanyaloglu@imperial.ac.uk](mailto:a.hanyaloglu@imperial.ac.uk)).

#### Materials Availability

All unique compounds and plasmids generated in this study are available upon request from the Lead Contact on a completed Materials Transfer Agreement.

#### Data and Code Availability

The datasets supporting the current study are available from the Lead Contact on request.

## METHODS

All methods can be found in the accompanying [Transparent Methods supplemental file](#).

## SUPPLEMENTAL INFORMATION

Supplemental Information can be found online at <https://doi.org/10.1016/j.isci.2020.101449>.

## ACKNOWLEDGMENTS

We would like to thank Drs. Andreas Bruckbauer and Stephen Rothery at the Facility for Imaging of Light Microscopy at Imperial College London for technical support with TIRFM and Dr. Paul Bech and Prof. Kevin Murphy (Imperial College London) for assistance with RIAs. FLAG-FFA3 plasmid was provided by Ms. Tilly Shackley (Imperial College London). This work was supported by grants from the Biotechnology and Biological Sciences Research Council to G.F., A.C.H., and E.T.W. (BB/N016947/1) and to A.H. and E.W.T. (BB/S001565/1). G.F. is supported by the Imperial College National Institute for Health Research (NIHR) Biomedical Research Centre (BRC) and NIHR Senior Investigator Award. A.I. was funded by LEAP (JP18gm0010004) from the Japan Agency for Medical Research and Development (AMED). The Facility for Imaging by Light Microscopy (FILM) at Imperial College London is part supported by funding from Biotechnology and Biological Sciences Research Council grant BB/L015129/1.

## AUTHOR CONTRIBUTIONS

Conceptualization, A.C.H. and G.F.; Methodology, N.C., N.G.-A., M.S., A.I., E.W.T.; Investigation and Formal Analysis, N.C., N.G.-A., and M.S.; Writing – Original Draft, N.C., N.G.-A., M.S., and A.C.H.; Writing – Review and Editing, N.C., N.G.-A., M.S., A.I., E.W.T., G.F., and A.C.H.; Funding Acquisition, A.I., E.T.W., G.F., and A.C.H.; Resources, A.I.; Supervision, E.T.W., G.F., and A.C.H.

## DECLARATION OF INTERESTS

The authors declare no competing interests.

Received: March 24, 2020

Revised: July 30, 2020

Accepted: August 10, 2020

Published: September 25, 2020

**REFERENCES**

- Alkhatib, G., Locati, M., Kennedy, P.E., Murphy, P.M., and Berger, E.A. (1997). HIV-1 coreceptor activity of CCR5 and its inhibition by chemokines: independence from G protein signaling and importance of coreceptor downmodulation. *Virology* 234, 340–348.
- Ang, Z., Xiong, D., Wu, M., and Ding, J.L. (2018). FFAR2-FFAR3 receptor heteromerization modulates short-chain fatty acid sensing. *FASEB J.* 32, 289–303.
- Aridor, M., Rajmilevich, G., Beaven, M.A., and Sagi-Eisenberg, R. (1993). Activation of exocytosis by the heterotrimeric G protein Gi3. *Science* 262, 1569–1572.
- Bolognini, D., Moss, C.E., Nilsson, K., Petersson, A.U., Donnelly, I., Sergeev, E., Konig, G.M., Kostenis, E., Kurowska-Stolarska, M., Miller, A., et al. (2016). A novel allosteric activator of free fatty acid 2 receptor displays unique Gi-functional bias. *J. Biol. Chem.* 291, 18915–18931.
- Brown, A.J., Goldsworthy, S.M., Barnes, A.A., Eilert, M.M., Tcheang, L., Daniels, D., Muir, A.I., Wigglesworth, M.J., Kinghorn, I., Fraser, N.J., et al. (2003). The Orphan G protein-coupled receptors GPR41 and GPR43 are activated by propionate and other short chain carboxylic acids. *J. Biol. Chem.* 278, 11312–11319.
- Caengprasad, N., and Hanyaloglu, A.C. (2019). Hardwiring wire-less networks: spatially encoded GPCR signaling in endocrine systems. *Curr. Opin. Cell Biol.* 57, 77–82.
- Calebiro, D., Nikolaev, V.O., Gagliani, M.C., De Filippis, T., Dees, C., Tacchetti, C., Persani, L., and Lohse, M.J. (2009). Persistent cAMP-signals triggered by internalized G-protein-coupled receptors. *PLoS Biol.* 7, e1000172.
- Chambers, E.S., Viardot, A., Psichas, A., Morrison, D.J., Murphy, K.G., Zac-Varghese, S.E., Maccougall, K., Preston, T., Tedford, C., Finlayson, G.S., et al. (2015). Effects of targeted delivery of propionate to the human colon on appetite regulation, body weight maintenance and adiposity in overweight adults. *Gut* 64, 1744–1754.
- Chambers, E.S., Byrne, C.S., Morrison, D.J., Murphy, K.G., Preston, T., Tedford, C., Garcia-Perez, I., Fountana, S., Serrano-Contreras, J.I., Holmes, E., et al. (2019). Dietary supplementation with inulin-propionate ester or inulin improves insulin sensitivity in adults with overweight and obesity with distinct effects on the gut microbiota, plasma metabolome and systemic inflammatory responses: a randomised cross-over trial. *Gut* 68, 1430–1438.
- Campbell, J.R., Martchenko, A., Sweeney, M.E., Maalouf, M.F., Psichas, A., Gribble, F.M., Reimann, F., and Brubaker, P.L. (2020). Essential role of syntaxin-binding protein-1 in the regulation of glucagon-like peptide-1 secretion. *Endocrinology* 161, bqaa039.
- Den Besten, G., Van Eunen, K., Groen, A.K., Venema, K., Reijngoud, D.J., and Bakker, B.M. (2013). The role of short-chain fatty acids in the interplay between diet, gut microbiota, and host energy metabolism. *J. Lipid Res.* 54, 2325–2340.
- Eichel, K., Jullie, D., and Von Zastrow, M. (2016).  $\beta$ -Arrestin drives MAP kinase signalling from clathrin-coated structures after GPCR dissociation. *Nat. Cell Biol.* 18, 303–310.
- Eichel, K., and Von Zastrow, M. (2018). Subcellular organization of GPCR signaling. *Trends Pharmacol. Sci.* 39, 200–208.
- Ferrandon, S., Feinstein, T.N., Castro, M., Wang, B., Bouley, R., Potts, J.T., Gardella, T.J., and Vilardaga, J.P. (2009). Sustained cyclic AMP production by parathyroid hormone receptor endocytosis. *Nat. Chem. Biol.* 5, 734–742.
- Fuller, M., Priyadarshini, M., Gibbons, S.M., Angueira, A.R., Brodsky, M., Hayes, M.G., Kovatcheva-Datchary, P., Bäckhed, F., Gilbert, J.A., Lowe, W.L., Jr., et al. (2015). The short-chain fatty acid receptor, FFA2, contributes to gestational glucose homeostasis. *Am. J. Physiol. Endocrinol. Metab.* 309, E840–E851.
- Gao, Z.G., and Jacobson, K.A. (2016). On the selectivity of the Galphai inhibitor UBO-QIC: a comparison with the Galphai inhibitor pertussis toxin. *Biochem. Pharmacol.* 107, 59–66.
- Ge, B., Gram, H., Di Padova, F., Huang, B., New, L., Ulevitch, R.J., Luo, Y., and Han, J. (2002). MAPKK-independent activation of p38alpha mediated by TAB1-dependent autophosphorylation of p38alpha. *Science* 295, 1291–1294.
- Gorvin, C.M., Rogers, A., Hastoy, B., Tarasov, A.I., Frost, M., Sposini, S., Inoue, A., Whyte, M.P., Rorsman, P., Hanyaloglu, A.C., et al. (2018). AP2? Mutations impair calcium-sensing receptor trafficking and signaling, and show an endosomal pathway to spatially direct G-protein selectivity. *Cell Rep.* 22, 1054–1066.
- Grimsey, N.J., Aguilar, B., Smith, T.H., Le, P., Soohoo, A.L., Puthenveedu, M.A., Nizet, V., and Trejo, J. (2015). Ubiquitin plays an atypical role in GPCR-induced p38 MAP kinase activation on endosomes. *J. Cell Biol.* 210, 1117–1131.
- Grundmann, M., Merten, N., Malfacini, D., Inoue, A., Preis, P., Simon, K., Ruttiger, N., Ziegler, N., Benkel, T., Schmitt, N.K., et al. (2018). Lack of beta-arrestin signaling in the absence of active G proteins. *Nat. Commun.* 9, 341.
- Hanyaloglu, A.C. (2018). Advances in membrane trafficking and endosomal signaling of G protein-coupled receptors. *Int. Rev. Cell Mol. Biol.* 339, 93–131.
- Hauge, M., Ekberg, J.P., Engelstoft, M.S., Timshel, P., Madsen, A.N., and Schwartz, T.W. (2017). Gq and Gs signaling acting in synergy to control GLP-1 secretion. *Mol. Cell. Endocrinol.* 449, 64–73.
- Hudson, B.D., Due-Hansen, M.E., Christiansen, E., Hansen, A.M., Mackenzie, A.E., Murdoch, H., Pandey, S.K., Ward, R.J., Marquez, R., Tikhonova, I.G., et al. (2013). Defining the molecular basis for the first potent and selective orthosteric agonists of the FFA2 free fatty acid receptor. *J. Biol. Chem.* 288, 17296–17312.
- Hudson, B.D., Tikhonova, I.G., Pandey, S.K., Ulven, T., and Milligan, G. (2012). Extracellular ionic locks determine variation in constitutive activity and ligand potency between species orthologs of the free fatty acid receptors FFA2 and FFA3. *J. Biol. Chem.* 287, 41195–41209.
- James, S.L., Muir, J.G., Curtis, S.L., and Gibson, P.R. (2003). Dietary fibre: a roughage guide. *Intern. Med. J.* 33, 291–296.
- Jean-Alphonse, F., Bowersox, S., Chen, S., Beard, G., Puthenveedu, M.A., and Hanyaloglu, A.C. (2014). Spatially restricted G protein-coupled receptor activity via divergent endocytic compartments. *J. Biol. Chem.* 289, 3960–3977.
- Komatsu, M., Schermerhorn, T., Aizawa, T., and Sharp, G.W. (1995). Glucose stimulation of insulin release in the absence of extracellular Ca<sup>2+</sup> and in the absence of any increase in intracellular Ca<sup>2+</sup> in rat pancreatic islets. *Proc. Natl. Acad. Sci. U S A* 92, 10728–10732.
- Kreft, M., Gasman, S., Chasserot-Golaz, S., Kuster, V., Rupnik, M., Sikdar, S.K., Bader, M., and Zorec, R. (1999). The heterotrimeric Gi(3) protein acts in slow but not in fast exocytosis of rat melanotrophs. *J. Cell Sci.* 112 (Pt 22), 4143–4150.
- Le Poul, E., Loison, C., Struyf, S., Springael, J.Y., Lannoy, V., Decobecq, M.E., Brezillon, S., Dupriez, V., Vassart, G., Van Damme, J., et al. (2003). Functional characterization of human receptors for short chain fatty acids and their role in polymorphonuclear cell activation. *J. Biol. Chem.* 278, 25481–25489.
- Lee, T., Schwandner, R., Swaminath, G., Weiszmann, J., Cardozo, M., Greenberg, J., Jaeckel, P., Ge, H., Wang, Y., Jiao, X., et al. (2008). Identification and functional characterization of allosteric agonists for the G protein-coupled receptor FFA2. *Mol. Pharmacol.* 74, 1599–1609.
- Li, M., Van Esch, B., Henricks, P.a.J., Folkerts, G., and Garssen, J. (2018). The anti-inflammatory effects of short chain fatty acids on lipopolysaccharide- or tumor necrosis factor alpha-stimulated endothelial cells via activation of GPR41/43 and inhibition of HDACs. *Front. Pharmacol.* 9, 533.
- Liou, A.P., Paziuk, M., Luevano, J.M., Jr., Machineni, S., Turnbaugh, P.J., and Kaplan, L.M. (2013). Conserved shifts in the gut microbiota due to gastric bypass reduce host weight and adiposity. *Sci. Transl. Med.* 5, 178ra41.
- Liu, S.H., Huang, Y.W., Wu, C.T., Chiu, C.Y., and Chiang, M.T. (2013). Low molecular weight chitosan accelerates glucagon-like peptide-1 secretion in human intestinal endocrine cells via a p38-dependent pathway. *J. Agric. Food Chem.* 61, 4855–4861.
- Mansvelter, H.D., Lodder, J.C., Sons, M.S., and Kits, K.S. (2002). Dopamine modulates exocytosis independent of Ca(2+) entry in melanotrophic cells. *J. Neurophysiol.* 87, 793–801.
- Mccluskey, A., Daniel, J.A., Hadzic, G., Chau, N., Clayton, E.L., Mariana, A., Whiting, A., Gorgani, N.N., Lloyd, J., Quan, A., et al. (2013). Building a better dynasore: the dyngo compounds potently inhibit dynamin and endocytosis. *Traffic* 14, 1272–1289.
- Miesenbock, G., De Angelis, D.A., and Rothman, J.E. (1998). Visualizing secretion and synaptic

transmission with pH-sensitive green fluorescent proteins. *Nature* 394, 192–195.

Nøhr, M.K., Pedersen, M.H., Gille, A., Egerod, K.L., Engelstoft, M.S., Husted, A.S., Sichlau, R.M., Grunddal, K.V., Poulsen, S.S., Han, S., et al. (2013). GPR41/FFAR3 and GPR43/FFAR2 as cosensors for short-chain fatty acids in enteroendocrine cells vs FFAR3 in enteric neurons and FFAR2 in enteric leukocytes. *Endocrinology* 154, 3552–3564.

Pingitore, A., Gonzalez-Abuin, N., Ruz-Maldonado, I., Huang, G.C., Frost, G., and Persaud, S.J. (2019). Short chain fatty acids stimulate insulin secretion and reduce apoptosis in mouse and human islets in vitro: role of free fatty acid receptor 2. *Diabetes Obes. Metab.* 21, 330–339.

Psichas, A., Sleeth, M.L., Murphy, K.G., Brooks, L., Bewick, G.A., Hanyaloglu, A.C., Ghatei, M.A., Bloom, S.R., and Frost, G. (2015). The short chain fatty acid propionate stimulates GLP-1 and PYY secretion via free fatty acid receptor 2 in rodents. *Int. J. Obes. (Lond.)* 39, 424–429.

Reimer, R.A. (2006). Meat hydrolysate and essential amino acid-induced glucagon-like peptide-1 secretion, in the human NCI-H716 enteroendocrine cell line, is regulated by extracellular signal-regulated kinase1/2 and p38 mitogen-activated protein kinases. *J. Endocrinol.* 191, 159–170.

Rutting, S., Xenaki, D., Malouf, M., Horvat, J.C., Wood, L.G., Hansbro, P.M., and Oliver, B.G. (2019). Short-chain fatty acids increase TNF $\alpha$ -induced inflammation in primary human lung mesenchymal cells through the activation of p38

MAPK. *Am. J. Physiol. Lung Cell Mol. Physiol.* 316, L157–L174.

Sato, Y., Nenquin, M., and Henquin, J.C. (1998). Relative contribution of Ca<sup>2+</sup>-dependent and Ca<sup>2+</sup>-independent mechanisms to the regulation of insulin secretion by glucose. *FEBS Lett.* 421, 115–119.

Sposini, S., Jean-Alphonse, F.G., Ayoub, M.A., Oqua, A., West, C., Lavery, S., Brosens, J.J., Reiter, E., and Hanyaloglu, A.C. (2017). Integration of GPCR signaling and sorting from very early endosomes via opposing APPL1 mechanisms. *Cell Rep.* 21, 2855–2867.

Spreckley, E., and Murphy, K.G. (2015). The L-cell in nutritional sensing and the regulation of appetite. *Front. Nutr.* 2, 23.

Takasaki, J., Saito, T., Taniguchi, M., Kawasaki, T., Moritani, Y., Hayashi, K., and Kobori, M. (2004). A novel Galphaq/11-selective inhibitor. *J. Biol. Chem.* 279, 47438–47445.

Tang, Z., Li, S., Han, P., Yin, J., Gan, Y., Liu, Q., Wang, J., Wang, C., Li, Y., and Shi, J. (2015). Pertussis toxin reduces calcium influx to protect ischemic stroke in a middle cerebral artery occlusion model. *J. Neurochem.* 135, 998–1006.

Thomsen, A.R.B., Jensen, D.D., Hicks, G.A., and Bunnett, N.W. (2018). Therapeutic targeting of endosomal G-protein-coupled receptors. *Trends Pharmacol. Sci.* 39, 879–891.

Tian, L., and Jin, T. (2016). The incretin hormone GLP-1 and mechanisms underlying its secretion. *J. Diabetes* 8, 753–765.

Tolhurst, G., Heffron, H., Lam, Y.S., Parker, H.E., Habib, A.M., Diakogiannaki, E., Cameron, J., Grosse, J., Reimann, F., and Gribble, F.M. (2012). Short-chain fatty acids stimulate glucagon-like peptide-1 secretion via the G-protein-coupled receptor FFAR2. *Diabetes* 61, 364–371.

Tsvetanova, N.G., and Von Zastrow, M. (2014). Spatial encoding of cyclic AMP signaling specificity by GPCR endocytosis. *Nat. Chem. Biol.* 10, 1061–1065.

Wheeler, S.E., Stacey, H.M., Nahaei, Y., Hale, S.J., Hardy, A.B., Reimann, F., Gribble, F.M., Larraufie, P., Gaisano, H.Y., and Brubaker, P.L. (2017). The SNARE protein syntaxin-1a plays an essential role in biphasic exocytosis of the incretin hormone glucagon-like peptide 1. *Diabetes* 66, 2327–2338.

Yonezawa, T., Kobayashi, Y., and Obara, Y. (2007). Short-chain fatty acids induce acute phosphorylation of the p38 mitogen-activated protein kinase/heat shock protein 27 pathway via GPR43 in the MCF-7 human breast cancer cell line. *Cell Signal.* 19, 185–193.

Yudowski, G.A., Puthenveedu, M.A., Leonoudakis, D., Panicker, S., Thorn, K.S., Beattie, E.C., and Von Zastrow, M. (2007). Real-time imaging of discrete exocytic events mediating surface delivery of AMPA receptors. *J. Neurosci.* 27, 11112–11121.

Zhang, J.-M., Sun, Y.-S., Zhao, L.-Q., Chen, T.-T., Fan, M.-N., Jiao, H.-C., Zhao, J.-P., Wang, X.-J., Li, F.-C., Li, H.-F., et al. (2019). SCFAs-induced GLP-1 secretion links the regulation of gut microbiome on hepatic lipogenesis in chickens. *Front. Microbiol.* 10, 2176.

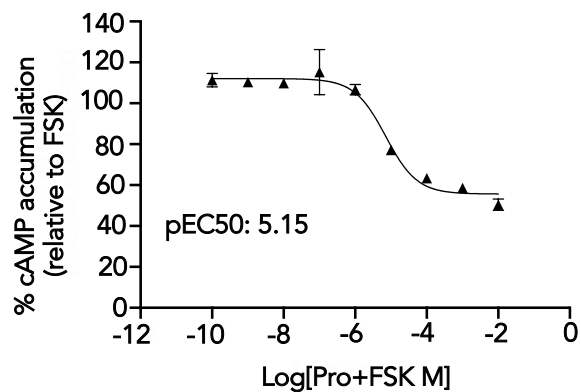
iScience, Volume 23

## **Supplemental Information**

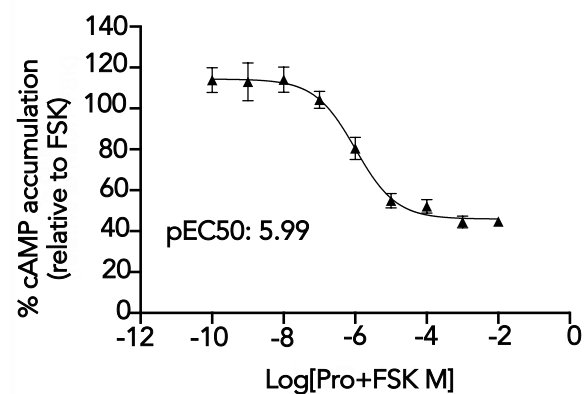
### **Internalization-Dependent Free Fatty Acid Receptor 2 Signaling Is Essential for Propionate- Induced Anorectic Gut Hormone Release**

**Natarin Caengprasath, Noemi Gonzalez-Abuin, Maria Shchepinova, Yue Ma, Asuka Inoue, Edward W. Tate, Gary Frost, and Aylin C. Hanyaloglu**

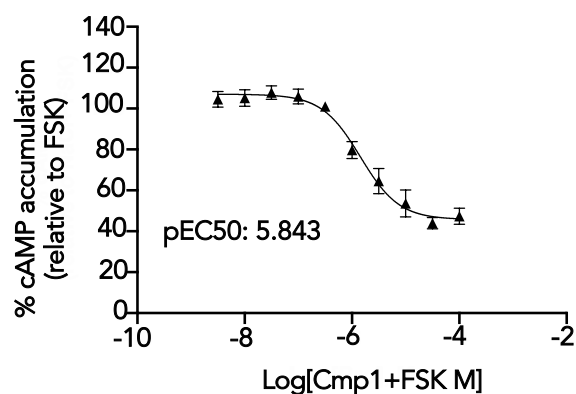
A



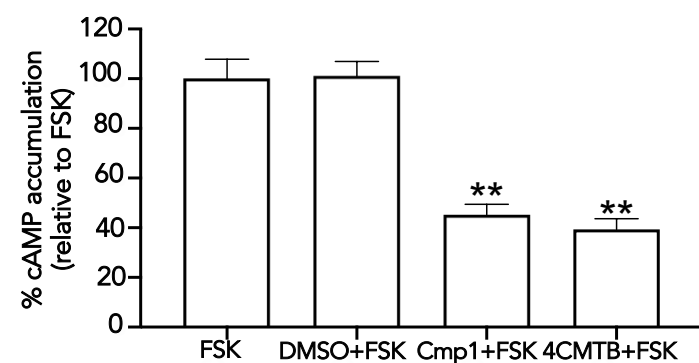
B



C

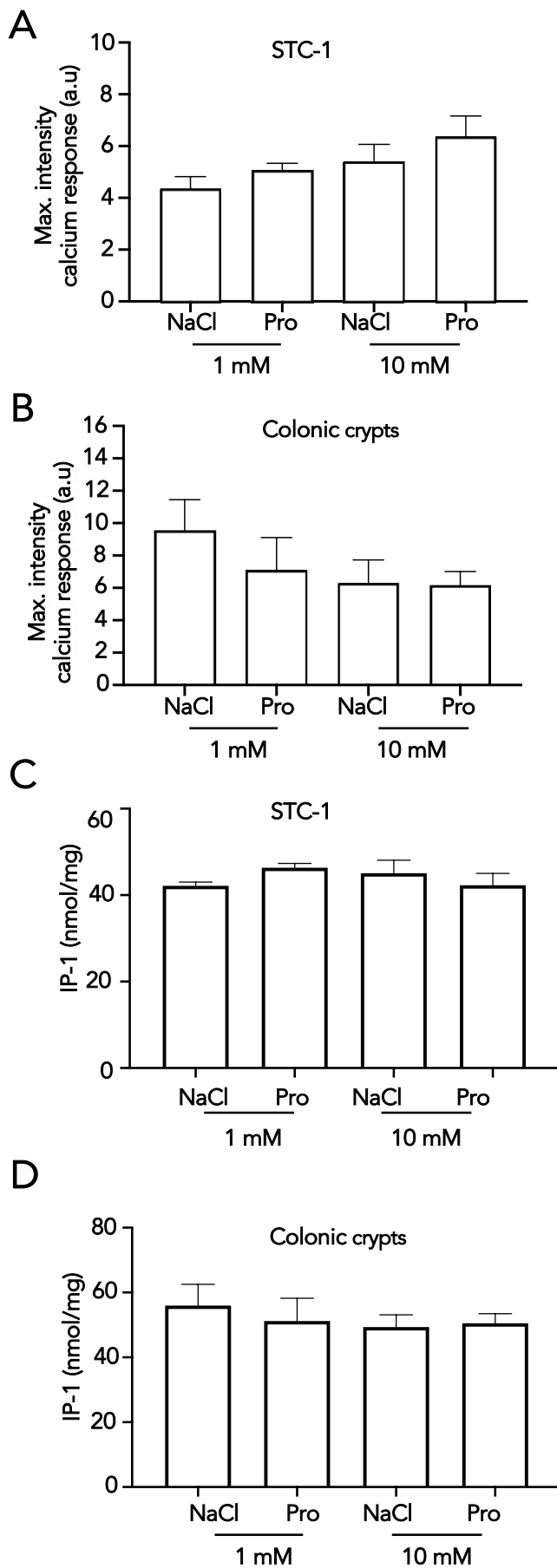


D

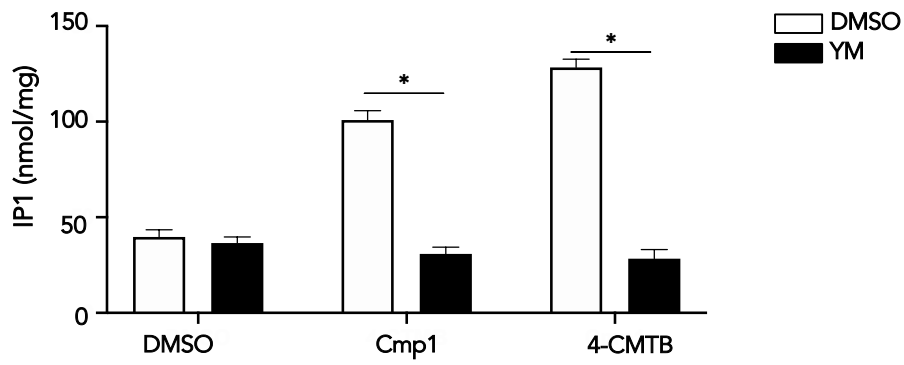


**Figure S1 Propionate and selective FFA2 ligands activates Gai/o signaling, related to Figure 1.** (A-B) Dose-response curves for propionate induced inhibition of forskolin induced cAMP signalling in STC-1 cells (A) and HEK 293 cells expressing FLAG-FFA2 (B). (C) Dose-response curve for the synthetic FFA2-selective ligand Compound 1 (Cmp1) in Flp-In™ T-Rex™ HEK 293 cells expressing FFA2-eYFP. n = 3 independent experiments. Data points shown are the mean ± SEM. (D) Gai/o signaling activated by FFA2 ligands was measured via inhibition of forskolin (FSK)-induced cAMP signaling in STC-1 cells. Cells were stimulated with either DMSO (untreated control), Compound 1 (Cmp1) or 4-CMTB (10uM, 5 min). n = 3 independent experiments. Two-sided Mann-Whitney U test, \*\*\* p < 0.001

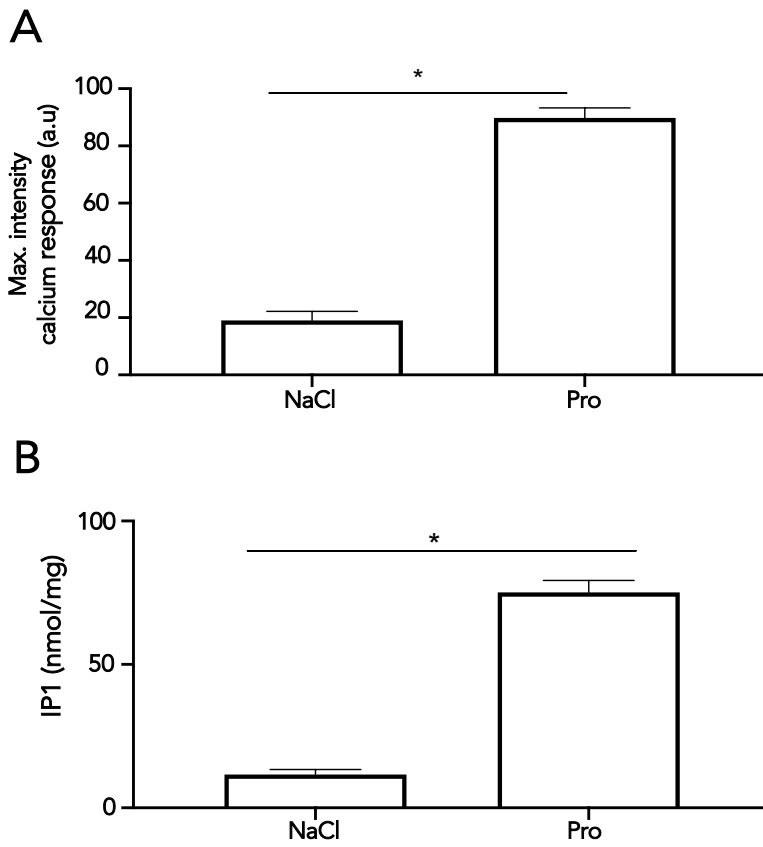




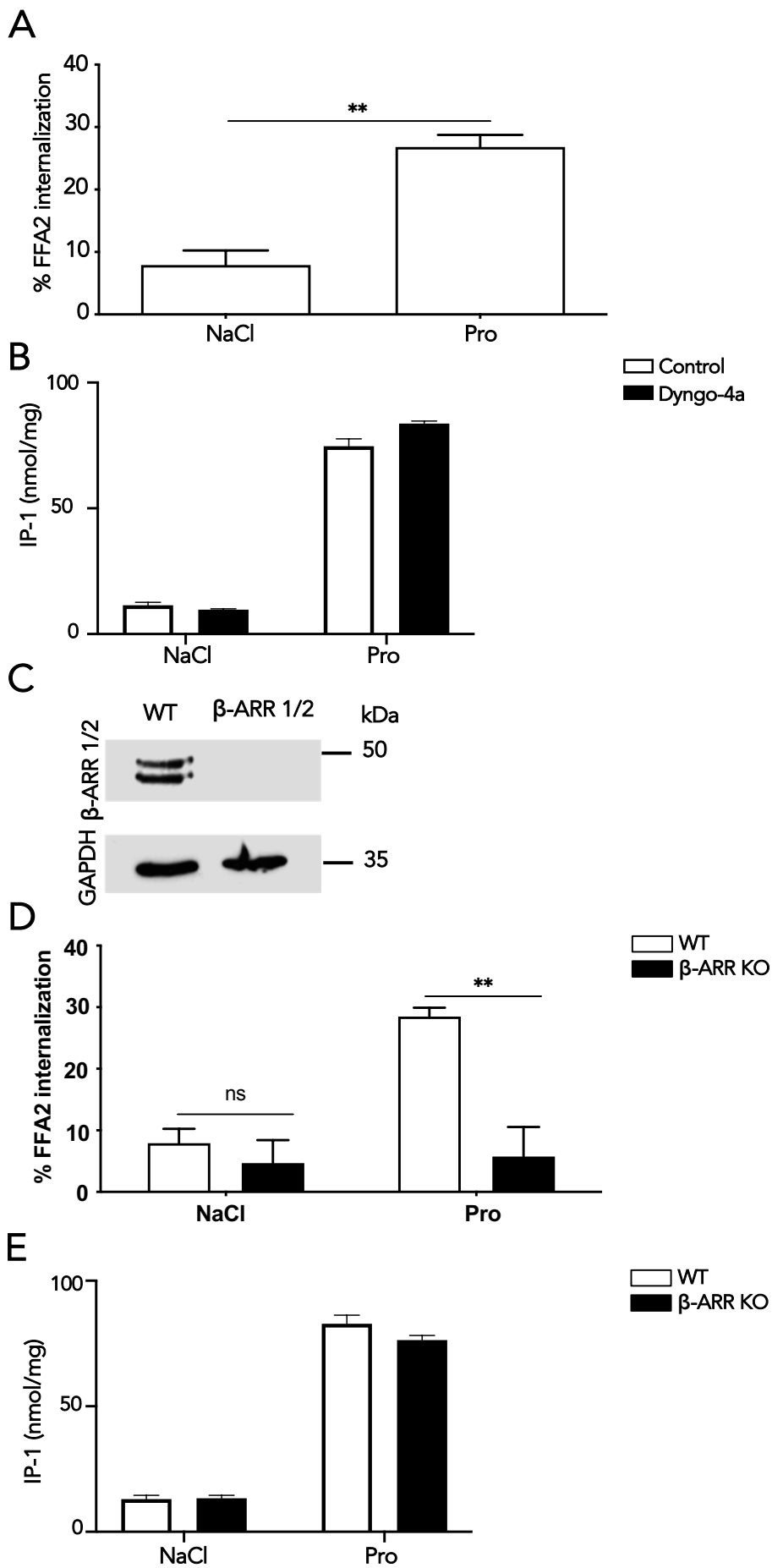
**Figure S2 High concentrations of propionate are unable to signal via Gαq/11 in enteroendocrine cells, related to Figure 1.** Intracellular calcium mobilization measured in STC-1 cells (A) or colonic crypts (B). Cultures were treated with either NaCl or sodium propionate (Pro) (1 and 10 mM). Average maximal intensities of  $n = 20$  cells in duplicate per 5 independent experiments. Two-sided Mann-Whitney U test. Data represent mean  $\pm$  SEM. Intracellular IP<sub>1</sub> levels measured in STC-1 cells (C) or colonic crypts (D). Cultures were treated with either NaCl sodium propionate (Pro) (1 and 10 mM). Two-sided Mann-Whitney U test. Data represent mean  $\pm$  SEM.



**Figure S3 FFA2-mediated IP<sub>1</sub> signaling requires active Gαq/11, related to Figure 1.** Intracellular IP<sub>1</sub> levels measured in STC-1 cells, pre-treated with YM-254890 (YM, 10 μM, 5 min) and stimulated with either DMSO (untreated control), Compound 1 (Cmp1) or 4-CMTB (10 μM, 5 min). n = 4 independent experiments. Two-sided Mann-Whitney U test, \*\*\* p < 0.001.

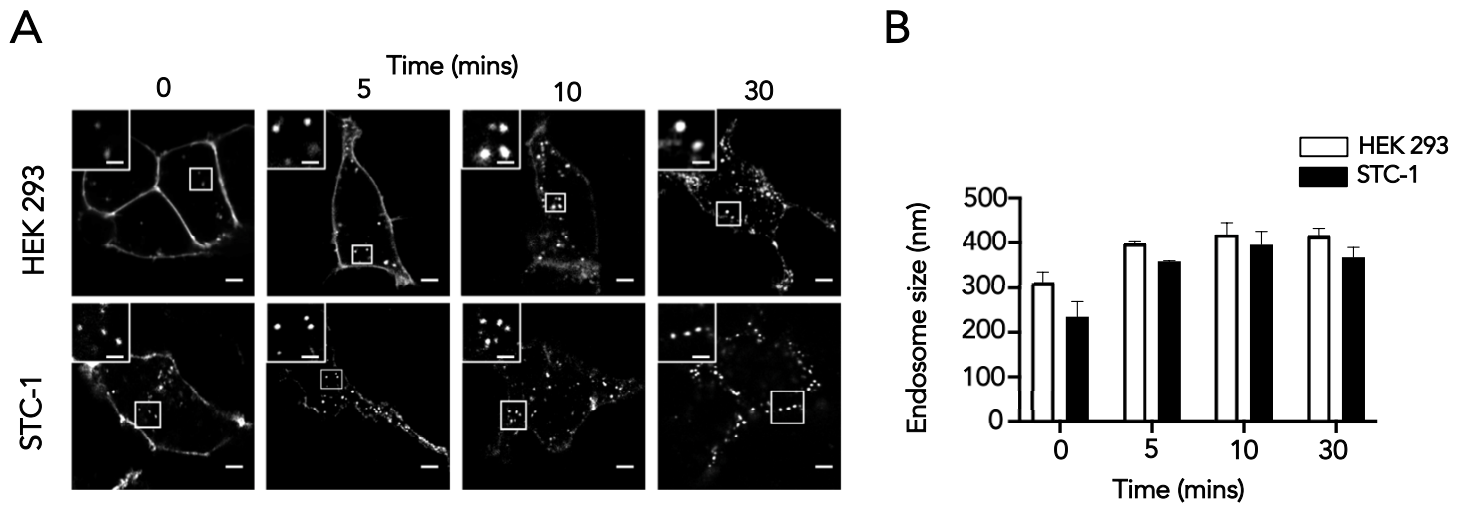


**Figure S4. FFA2 activates both Gai/o and Gq $\alpha$ /11 signaling in HEK 293 cells, related to Figure 1.** Intracellular calcium mobilization (A) or intracellular accumulation of IP<sub>1</sub> (B) measured in HEK 293 cells expressing FLAG-FFA2. Cells were stimulated with either NaCl or sodium propionate (Pro) (1 mM). For intracellular calcium mobilization, average maximal intensities of n = 20 cells in duplicate per 4 independent experiments. Two-sided Mann-Whitney U test, \* p < 0.05. For IP<sub>1</sub>, n = 4 independent experiments. Two-sided Mann-Whitney U test, \*\*\* p < 0.00. Data represent mean  $\pm$  SEM.



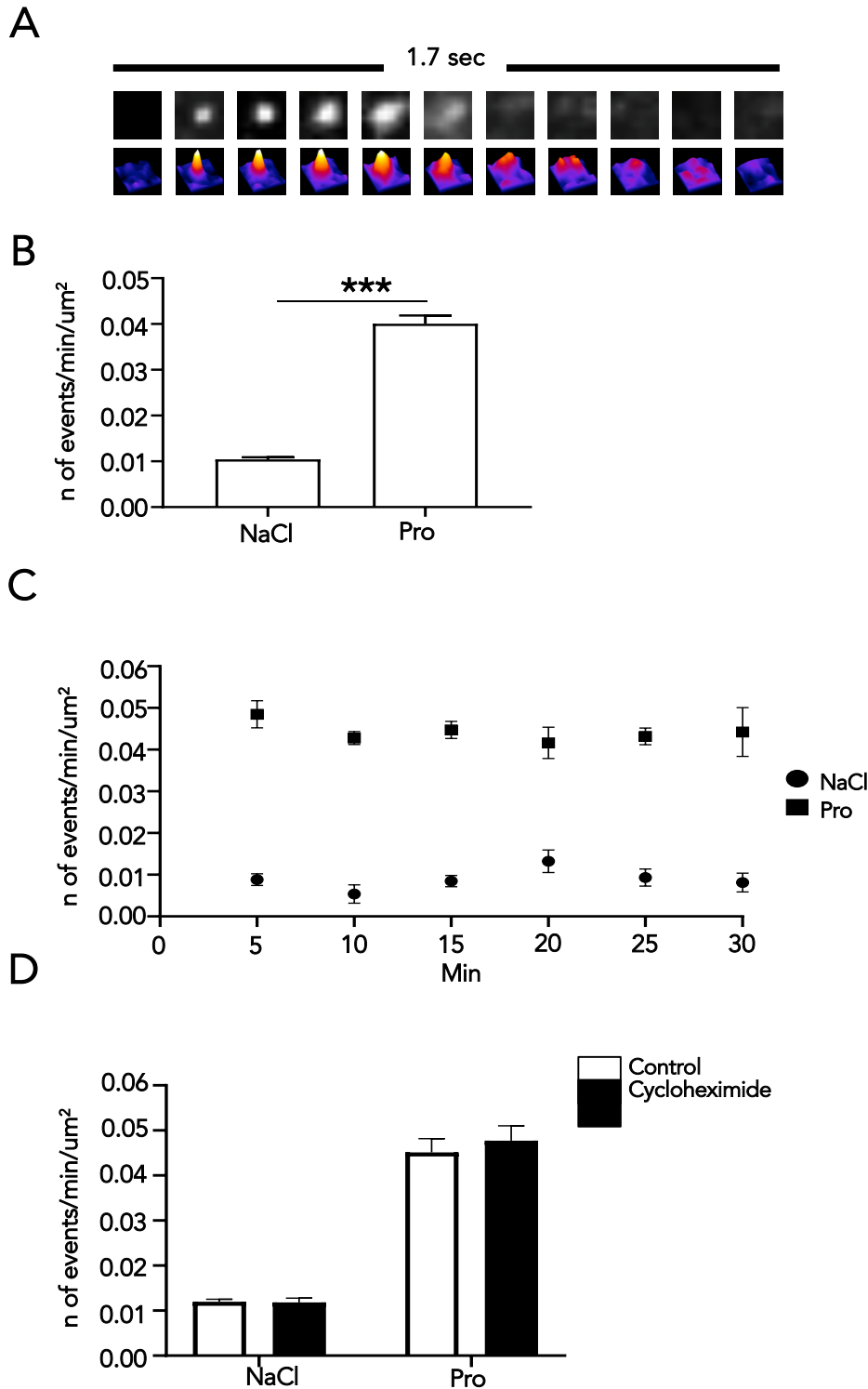
**Figure S5 Differential spatial requirement for FFA2-mediated signaling, related to Figure 2.** (A) FFA2 internalization measured by flow cytometry. HEK 293 cells transiently expressing FLAG-FFA2 were treated with and without NaCl (1 mM), or sodium propionate (Pro) (1 mM, 20 mins). FFA2 internalization was determined by decrease cell-surface labeling compared to untreated control.  $n = 4$  independent experiments. Two-sided Mann-Whitney U test,  $** p < 0.01$ . (B) Intracellular accumulation of IP<sub>1</sub> measured in HEK 293 cells transiently expressing FLAG-FFA2 pre-treated with either DMSO (vehicle) or Dyngo-4a (50  $\mu$ M, 45 min) and treated with either NaCl or propionate (Pro) (1 mM, 2 h).  $n = 4$  independent experiments. Two-sided Mann-Whitney U test. (C) Western blot confirmation of the absence of  $\beta$ -arrestin 1/2

( $\beta$ -ARR) expression in  $\beta$ -ARR KO HEK 293 cells compared to WT cells. GAPDH was used as loading control. (D) Dependence of FFA2 internalization on  $\beta$ -ARR measured by flow cytometry. WT and  $\beta$ -ARR KO HEK 293 cells transiently expressing FLAG-FFA2 were treated and data analysis were carried as in (A).  $n = 4$  independent experiments. Two-sided Mann-Whitney U test, \*\*  $p < 0.01$ . (E) Intracellular accumulation of  $IP_1$  measured in WT or  $\beta$ -ARR KO transiently expressing FLAG-FFA2 cells and treated as in (B).  $n = 24$  independently plated wells for either WT or  $\beta$ -ARR KO transiently expressing FLAG-FFA2, representative of 4 independent experiments. Two-sided Mann-Whitney U test. Data represent mean  $\pm$  SEM.

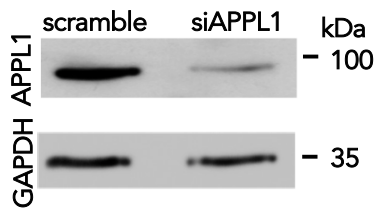


**Figure S6 FFA2 internalizes to endosomes exhibiting properties of VEEs, related to Figure 3.** (A) (i) Representative confocal microscopy images of STC-1 or HEK 293 cells transiently expressing FLAG-FFA2 imaged live via confocal microscopy before and after propionate treatment at different time points (1 mM). (ii) Bar graph showing diameter of FFA2 containing endosomes in HEK 293 or STC-1 cells. Endosome diameter was assessed by measuring the diameter of 20 endosomes, n = 10 cells per condition, collected across 3 independent experiments.

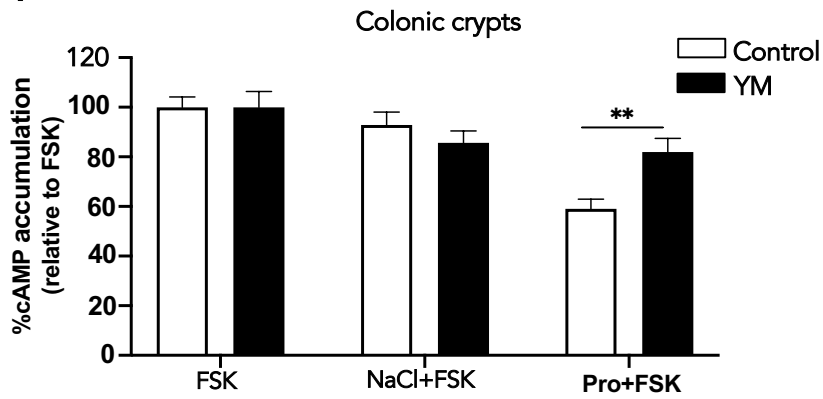
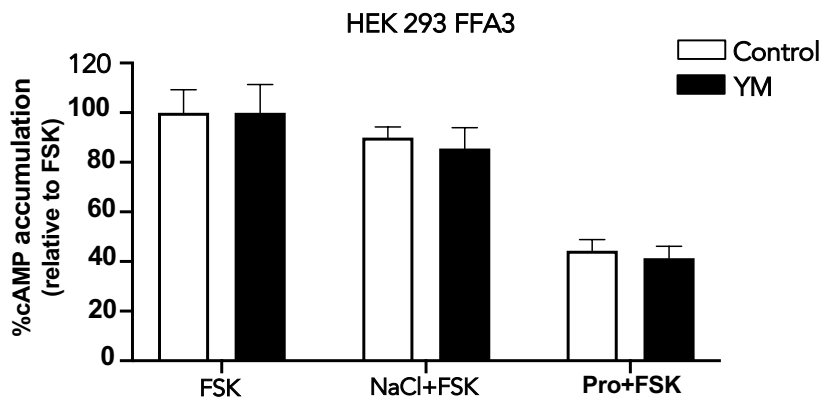




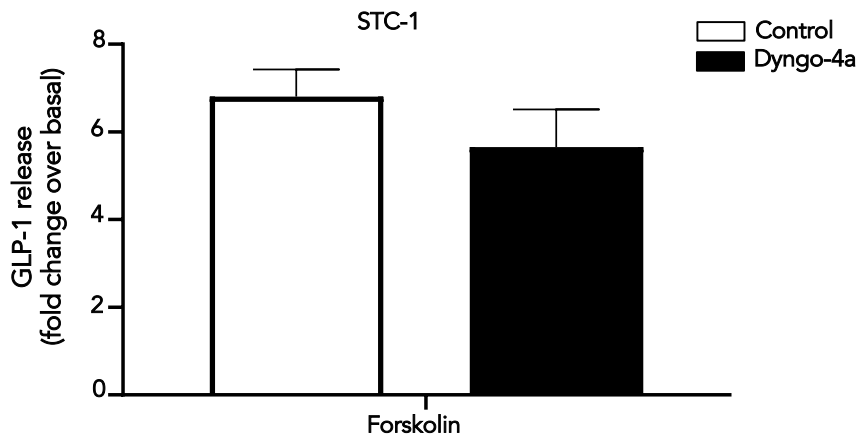
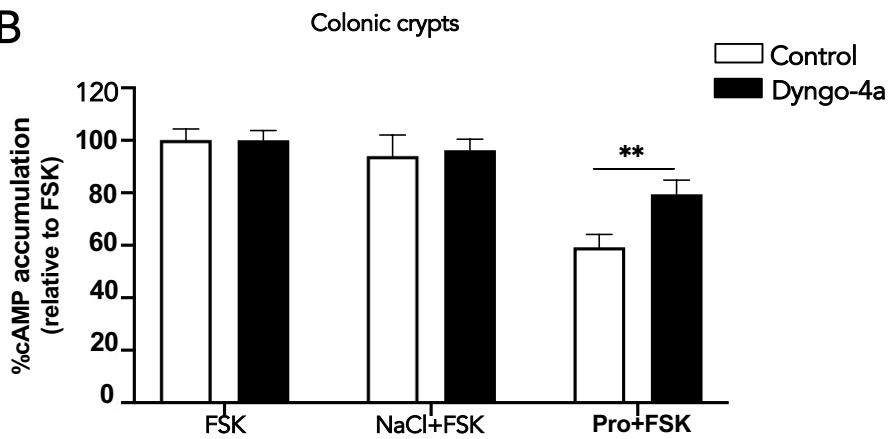
**Figure S7 Characterization of SEP-FFA2 recycling events via TIRFM, related to Figure 4.** (A) Series of TIRFM images of a single SEP-FFA2 recycling event following propionate stimulation with surface plot of fluorescence. (B) Number of recycling events measured by TIRFM in HEK 293 cells stably expressing SEP-FFA2 following stimulation of NaCl (1 mM) or propionate (Pro) (1 mM);  $n = 15$  cells per condition; collected across 3 independent experiments. Two-sided Mann-Whitney U test, \*\*\*  $p < 0.001$ . (C) Number of recycling events over time following stimulation of NaCl (1 mM) or propionate (Pro) (1 mM) measured by TIRFM in HEK 293 cells stably expressing SEP-FFA2;  $n = 4$  cells per time point; collected across 3 independent experiments. (D) Number of recycling events measured by TIRFM in HEK 293 cells stably expressing SEP-FFA2, pre-treated with DMSO (vehicle) or cycloheximide (10  $\mu\text{g}/\text{mL}$ , 90 minutes) prior to NaCl (1 mM) or propionate (Pro) (1 mM) stimulation.  $n = 10$  cells per condition, collected across 3 independent experiments. Two-sided Mann-Whitney U test. Data represent mean  $\pm$  SEM.



**Figure S8 APPL1 knockdown in STC-1 cells via siRNA, related to Figure 4.** Representative western blot of total cellular levels of APPL1 in lysates collected from STC-1 following either scramble (control), APPL1 (siAPPL1) siRNA-mediated knockdown. GAPDH was used as loading control.

**A****B**

**Figure S9** The Gαq/11 inhibitor, YM-254890, partially inhibits Gai/o signaling activated by propionate/FFA2, related to **Figure 5**. (A) Gai/o signaling activated by propionate (Pro) (1 mM, 5 min) in colonic crypts was measured via inhibition of forskolin (FSK)-induced cAMP signaling and pre-treated with or without YM-254890 (YM, 5 min, 10 mM). n = 4 independent experiments. Two-sided Mann-Whitney U test, \*\*, p < 0.01. (B) HEK 293 cells transiently expressing FFA3, was pre-treated with and without YM, and Gai/o signaling measured as in (A). n = 4 independent experiments. Two-sided Mann-Whitney U test, \*\*, p < 0.01. Data represent mean ± SEM.

**A****B**

**Figure S10 Dyngo-4 partially inhibits Gai/o signaling activated by propionate/FFA2 in colonic crypts, related to Figure 5.** (A) Forskolin induced GLP-1 release from STC-1 cells in the presence of Dyngo-4a. STC-1 cells were pre-treated with either DMSO or Dyngo-4a (50  $\mu$ M, 45 min).  $n = 5$  independent experiments. Two-sided Mann-Whitney U test. (B) Gai/o signaling activated by propionate (Pro) (1 mM, 5 min) in colonic crypts was measured via inhibition of forskolin (FSK)-induced cAMP signaling and pre-treated with or without Dyngo-4a (50  $\mu$ M, 45 min).  $n = 4$  independent experiments. Two-sided Mann-Whitney U test, \*\*,  $p < 0.01$ . Data represent mean  $\pm$  SEM.

## Transparent methods

### Animals

C57BL/6J male mice purchased from Charles River were used to prepare mouse colonic crypts. FFA2 global knockout (FFA2<sup>-/-</sup>) male mice were generated by Deltagen. FFA2 knockout was achieved by homologous recombination that replaces 55bp of FFA2 exon 1 with a cassette containing the neomycin resistance and  $\beta$ -galactosidase genes, resulting in a frameshift mutation (Maslowski et al., 2009). Animals were cared for in accordance with the British Home Office under UK Animal (Scientific Procedures) Act 1986 (Project License 00/6474).

### Mouse colonic crypt culture preparation

Colons of wildtype (WT) or FFA2<sup>-/-</sup> C57BL6 mice (8-12 weeks of age) were removed, cleaned and placed into ice-cold L-15 (Leibowitz) medium (Sigma). The intestinal tissue was thoroughly cleaned with L-15 medium and digested with 0.4 mg ml<sup>-1</sup> collagenase (Sigma) in high-glucose DMEM at 37°C, as described previously (Psichas et al., 2015). The digestion process was repeated 4 times and resulting cell suspensions were centrifuged (5 min, 300 x g). The pellets were resuspended in DMEM (supplemented with 10% FBS and 1% antibiotics (100 U ml<sup>-1</sup> penicillin and 0.1 mg ml<sup>-1</sup> streptomycin)). Combined cell suspensions were filtered through a nylon mesh (pore size ~250  $\mu$ m) and plated onto appropriate culture plates with wells coated with 2% Matrigel (Corning). The plates were incubated overnight at 37°C in an atmosphere of 95% O<sub>2</sub> and 5% CO<sub>2</sub>.

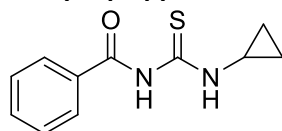
### Colonic crypt FFA3 mRNA expression levels

Total RNA was extracted from plated WT and FFA2<sup>-/-</sup> (age-matched) colonic crypts using PureLink® RNA Mink Kit (Invitrogen) and DNase treated using on-column PureLink® DNase Treatment (Invitrogen). DNase-treated total RNA was reversed transcribed to a single-stranded cDNA using the high-capacity cDNA Reverse Transcription kit (Applied Biosystems). Quantitative reverse transcriptase PCR (qPCR) was carried out by QuantStudio® 12 K Flex Real-Time PCR System (Life Technologies) using TaqMan Gene Expression Assay (Applied Biosystems) with FFAR3 hydrolysis probe (Mm02621638\_1, Applied Biosystems) and 18S as the reference gene (Eukaryotic 18S rRNA Endogenous Control, Applied Biosystems). The qPCR data are presented as relative expression levels calculated by  $\Delta\Delta C_t$  (where  $\Delta C_t$  is determined by the difference cycles threshold of the target gene and the reference gene).

### Synthesis of Compound 1

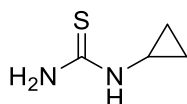
All solvents and reagents were purchased from Sigma-Aldrich, Alfa Aesar unless otherwise stated, and used without further purification. Moisture sensitive reactions were performed in oven dried flasks, under a nitrogen atmosphere. Anhydrous solvents were dispensed using Pure Solv™ solvent drying towers (Innovative Technology Inc.) Analytical thin layer chromatography was carried out using Merck Si<sub>60</sub>, F<sub>254</sub> chromatography sheets. Spots were visualised by UV light or through use of an appropriate stain (ninhydrin or potassium permanganate). Flash column chromatography was run on a Biotage Isolera™ One flash purification system using a wet-loading Biotage SNAP cartridge. Mass spectra were acquired by the Imperial Mass Spectrometry service with *m/z* values reported in Daltons. <sup>1</sup>H spectra were recorded on a Bruker Av-400 (400 Hz) instrument at RT. Chemical shifts are expressed in parts per million  $\delta$  relative to residual solvent as an internal reference. The multiplicity if each signal is indicated by: s = singlet; broad s = broad singlet; d = doublet; t = triplet; m = multiplet. Coupling constants (*J*), calculated using MestReNova® NMR software, are quoted in Hz and recorded to the nearest 0.1 Hz.

### 1 *N*-cyclopropyl-*N'*-benzoylthiourea



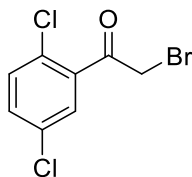
Benzoyl isothiocyanate (820  $\mu$ L, 6.13 mmol, 1.0 eq.) was dissolved in CH<sub>2</sub>Cl<sub>2</sub> (25 mL) at 0 °C, followed by a dropwise addition of cyclopropylamine (425  $\mu$ L, 6.13 mmol, 1.0 eq.). The solution was then warmed up to RT and allowed to stir for 17h. The crude mixture was concentrated *in vacuo*, yielding benzoylthiourea as a yellow solid (1348 mg, quant.), which was used in the next step without further purification. <sup>1</sup>H NMR (400 MHz, CDCl<sub>3</sub>):  $\delta$  10.93 (1H, broad t), 9.17 (1H, s), 7.83 (2H, dd, *J* = 8.4, 1.4 Hz), 7.59 (1H, t, *J* = 7.4 Hz), 7.48 (2H, t, *J* = 7.9 Hz), 3.23-3.17 (1H, m), 0.93-0.89 (2H, m), 0.80-0.77 (2H, m). The compound has been characterized in the literature, data in agreement (Olken and Marletta, 1992).

### 2 Cyclopropylthiourea



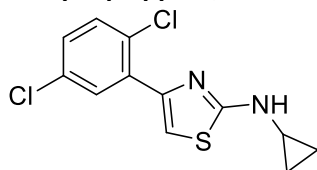
Benzoylthiourea **1** (900 mg, 4.09 mmol, 1 eq.) was dissolved in a solution of 5% (w/v) NaOH (20 mL) and heated to 80 °C. The solution was stirred for 3h and then cooled to RT in an ice/water bath. The reaction mixture was titrated to pH 8.0 with HCl<sub>conc</sub>. The crude was extracted with EtOAc (4 x 15 mL). The organic fractions were combined, dried over anhydrous MgSO<sub>4</sub>, filtered and concentrated *in vacuo*. The crude was redissolved in CH<sub>2</sub>Cl<sub>2</sub> (10 mL) and precipitated with a dropwise addition of Et<sub>2</sub>O to afford a thiourea **2** as a white-off solid (200 mg, 42%), which was used in the next step without further purification. <sup>1</sup>H NMR (400 MHz, DMSO-*d*<sub>6</sub>): δ 2.35 (1H, broad s), 0.67-0.63 (2H, m), 0.49-0.44 (2H, m). The compound has been characterized in the literature, data in agreement (Olken and Marletta, 1992).

### 3 2-Bromo-1-(2,5-dichlorophenyl)ethanone



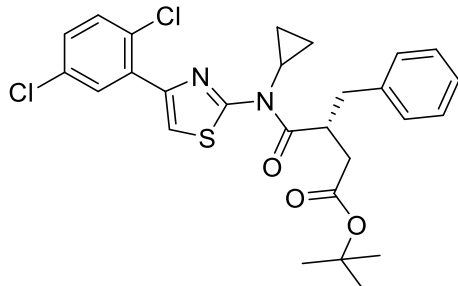
Dichloroacetophenone (230 μL, 1.59 mmol, 1.0 eq.) was dissolved in anhydrous MeCN (8 mL) and cooled to 0 °C under nitrogen, then NBS (312 mg, 1.75 mmol, 1.1 eq.) was added, followed by a dropwise addition of TMS-OTf (14 μL, 0.08 mmol, 0.05 eq.). The solution was warmed up to RT and allowed to stir for 17h under nitrogen. The reaction mixture was concentrated *in vacuo* and purified by column chromatography (1 to 5% EtOAc in Hexane over 10 CV), which afforded bromide as a white-off thick oil (235 mg, 55%, 80% pure by NMR). <sup>1</sup>H NMR (400 MHz, CDCl<sub>3</sub>): δ 7.54 (1H, d, *J* = 2.4 Hz), 7.40 (1H, d, *J* = 2.3 Hz), 7.39 (1H, s), 4.49 (2H, s). The compound has been characterized in the literature, data in agreement (Roman et al., 2010).

### 4 N-cyclopropyl-4-(2,5-dichlorophenyl)thiazol-2-amine



Cyclopropylthiourea **2** (50 mg, 0.43 mmol, 1.0 eq.) was dissolved in ethanol (2 mL), followed by addition of bromide **3** (80% pure, 138 mg, 0.52 mmol, 1.2 eq.) pre-dissolved in ethanol (1 mL). The solution was allowed to stir for 3h at RT and then concentrated *in vacuo*. The residue was dissolved in CH<sub>2</sub>Cl<sub>2</sub> (5 mL), washed with saturated NaHCO<sub>3</sub> (4 mL), brine (4 mL). Organic layer was dried over MgSO<sub>4</sub>, filtered and concentrated *in vacuo* to give a thick yellow oil. Column chromatography (1 to 10% EtOAc in Hexane over 10 CV) afforded amine **4** as an off-white thick oil (92 mg, 75%). *R*<sub>f</sub> 0.57 (Hex:EtOAc = 3:1). <sup>1</sup>H NMR (400 MHz, CDCl<sub>3</sub>): δ 7.86 (1H, d, *J* = 2.6 Hz), 7.37 (1H, d, *J* = 8.4 Hz), 7.19 (1H, dd, *J* = 8.3, 2.8 Hz), 7.13 (1H, broad s), 7.08 (1H, s), 2.60-2.54 (1H, m), 0.69-0.64 (2H, m), 0.56-0.52 (2H, m). The compound has been characterized in the literature, data in agreement (Hoveyda et al., 2018).

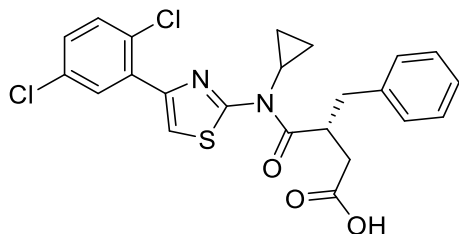
### 5 tert-Butyl (R)-3-benzyl-4-(cyclopropyl(4-(2,5-dichlorophenyl)thiazol-2-yl)amino)-4-oxobutanoate



In a dry microwave vial (R)-2-benzyl-4-(tert-butoxy)-4-oxobutanoic acid (30 mg, 0.114 mmol, 1.3 eq.) was dissolved in anhydrous CH<sub>2</sub>Cl<sub>2</sub> (1 mL) under nitrogen. Fluoro-*N,N,N',N'*-bis(tetramethylene)formamidinium hexafluorophosphate (BTFFH) (41 mg, 0.131 mmol, 1.5 eq.) was then added, followed by anhydrous *i*-Pr<sub>2</sub>NEt (68 μL, 0.391 mmol, 4.5 eq.). The solution was allowed to stir for 30 min at RT under nitrogen, followed by addition of amine **4** (25 mg, 0.088 mmol, 1.0 eq.). The vial was then sealed, heated to 80 °C in an oil bath and allowed to stir for 18h. The yellow reaction mixture was cooled down to RT, further diluted with CH<sub>2</sub>Cl<sub>2</sub> (5 mL), quenched with saturated NH<sub>4</sub>Cl (4 mL), washed with H<sub>2</sub>O (4 mL) and brine (4 mL). The organic layer was dried over anhydrous

MgSO<sub>4</sub>, filtered and concentrated *in vacuo* to give a dark-yellow thick oil. Column chromatography (1 to 10% EtOAc in Hexane over 10 CV) afforded amide **5** as a light-yellow thick oil (37 mg, 78%). R<sub>f</sub> 0.65 (Hex:EtOAc = 3:1). <sup>1</sup>H NMR (400 MHz, CDCl<sub>3</sub>): δ 7.99 (1H, d, *J* = 2.8 Hz), 7.62 (1H, s), 7.39 (1H, d, *J* = 8.6 Hz), 7.30-7.15 (6H, m), 4.23-4.13 (1H, m), 3.08 (1H, dd, *J* = 13.4, 6.7 Hz), 2.96-2.82 (2H, m), 2.73 (1H, dd, *J* = 13.4, 8.2 Hz), 2.44 (1H, dd, *J* = 16.4, 4.9 Hz), 1.39 (9H, s), 1.30-1.20 (3H, m), 0.85-0.78 (1H, m). LRMS (ES<sup>+</sup>): 531 ([<sup>35</sup>Cl<sub>35</sub>CIM+H]<sup>+</sup>, 100%), 533 ([<sup>35</sup>Cl<sup>37</sup>CIM+H]<sup>+</sup>, 75%), 535 ([<sup>37</sup>Cl<sup>37</sup>CIM+H]<sup>+</sup>, 20%). The compound has been characterized in the literature, data in agreement (Hoveyda et al., 2018).

#### 6 (R)-3-benzyl-4-(cyclopropyl(4-(2,5-dichlorophenyl)thiazol-2-yl)amino)-4-oxobutanoic acid (Cmp1)



Amide **5** (10 mg, 0.019 mmol, 1.0 eq.) was dissolved in anhydrous CH<sub>2</sub>Cl<sub>2</sub> (180 mL) under nitrogen, followed by addition of TFA<sub>conc</sub> (40 mL, 20% (v/v)). The solution was allowed to stir for 4h at RT. The reaction mixture was concentrated *in vacuo*, redissolved in CH<sub>2</sub>Cl<sub>2</sub> (3 mL) and quenched with saturated NaHCO<sub>3</sub> (3 mL). The organic layer was dried over anhydrous MgSO<sub>4</sub>, filtered and concentrated *in vacuo*. The residue was redissolved in CH<sub>2</sub>Cl<sub>2</sub> (3 mL) and precipitated with a dropwise addition of Et<sub>2</sub>O to afford **Cmp1** as a beige powder (4.6 mg, 51%). The compound is unstable in solution under non-anhydrous conditions and decomposes to starting materials. The 10 mM stock of **Cmp1** in DMSO was immediately aliquoted and kept frozen at -20 °C. <sup>1</sup>H NMR (400 MHz, DMSO-*d*<sub>6</sub>): δ 7.96 (1H, d, *J* = 2.7 Hz), 7.82 (1H, broad s), 7.61 (1H, d, *J* = 8.7 Hz), 7.47 (1H, dd, *J* = 8.4, 2.6 Hz), 7.32-7.14 (5H, m), 4.16-4.02 (1H, m), 3.07-2.81 (2H, m), 2.80-2.61 (2H, m), 2.38 (1H, d, *J* = 2.40 Hz), 1.28-1.16 (3H, m), 0.85-0.74 (1H, m). LRMS (ES<sup>+</sup>): 475 ([<sup>35</sup>Cl<sub>35</sub>CIM+H]<sup>+</sup>, 100%), 477 ([<sup>35</sup>Cl<sup>37</sup>CIM+H]<sup>+</sup>, 75%), 479 ([<sup>37</sup>Cl<sup>37</sup>CIM+H]<sup>+</sup>, 20%). The compound has been characterized in the literature, data in agreement (Hoveyda et al., 2018).

#### Plasmids

FLAG-FFA2 was generated by amplification of mouse FFA2 plasmid (MC203984, Origene) with forward 5'-GCTGATGACCCCAGACTGGCACAG-3' and reverse 5'-GCTCTAGACTACTCGGTGACAAATTCAGAACTCTG-3' primers and was ligated into XbaI and AfeI sites of the FLAG-LHR/pcDNA3.1 via digestion. SEP-FFA2 was generated by subcloning SEP from SEP-LHR using XbaI and AfeI sites and ligated to FFA2. FFA2-eYFP was generated by the amplification of mouse FFA2 (pFN21A Halo-mFFA2, Promega, UK) with forward 5'-cagcctccggactctagcgtgccATGACCCCAGACTGGCAC-3' and reverse 5'-tgccgccgccctcCGGTGACAAATTCAGAACTC-3' primers that was fused with enhanced yellow fluorescent protein (eYFP) by the amplification of eYFP plasmid (expression vector pC1-mEYFP, in-house plasmid) with forward 5'-tgtcaccgagggcgccgcgccgagcGTGAGCAAGGGCGAGGAGC-3' and reverse 5'-tagaaggcacagctcagggctctaCTTGACAGCTCGTCCATGC-3' primers. Amplified FFA2 and eYFP were inserted into linearized pcDNA5/FRT/TO plasmid (kindly provided by A. Tavassoli, G. Schmalzing and M. Rosenkilde labs) (forward 5'-tagAGCCTCGACTGTGCCTC-3' and reverse 5'-ggcACGCTAGAGTCCGGAGGC-3' primers) using NEBuilder® HIFI DNA Assembly Master Mix (New England Biolabs). FLAG-LHR and SEP-LHR have been previously described (Jean-Alphonse et al., 2014; Sposini et al., 2017), respectively. FLAG-β2AR was a kind gift from Mark Von Zastrow, UCSF. Gαi-Venus was a kind gift from Johnathan Javitch, Columbia University. Gβ and Gγ were a kind gift from Eric Reiter, INRA, Nouzilly.

#### Cell Culture, transfections and stable cell lines

STC-1 (ATCC, male) and WT (ATCC) or β-ARR 1/2 KO (Asuka Inoue) HEK 293 cells (female) were maintained in high-glucose DMEM containing 10% FBS and penicillin/streptomycin (100 U/mL) at 37°C in 5% CO<sub>2</sub>. Flp-In TREx HEK 293 cells (Francis Crick Institute) were maintained in high-glucose DMEM containing 10% FBS, 15 μg/mL blasticidin and 100 μg/mL zeocin at 37°C in 5% CO<sub>2</sub>. For STC-1 or HEK 293 cells, transient transfections of plasmids were performed using Lipofectamine 2000 (Invitrogen) and cells were assayed 72 h post-transfection. Transfection of siRNA scramble or siRNA APPL1 (HSS119758, Life Technologies) was performed using RNAiMAX (Invitrogen) and cells were assayed 96 h post-transfection. To generate FLAG-FFA2 and SEP-FFA2 stable cell lines, FLAG- or SEP- FFA2 was transfected in HEK 293 cells using Lipofectamine 2000 with cells cultured in the presence of 0.5 μg/mL of geneticin. Geneticin-resistant clones were screened for receptor expression by flow cytometry and confocal microscopy. To generate Flp-In TREx HEK 293 cells able to inducibly express FFA2-eYFP, cells were cotransfected with pOG44 complementary vector and pcDNA5/FRT/TO-mFFA2-eYFP (9:1) using Lipofectamine 2000 with cells cultured in the presence of 100 μg/mL of hygromycin B to initiate selection of stably transfected cells. Following isolation of resistant cells, expression of FFA2-eYFP was induced by treatment with 1 μg/mL tetracycline one day prior to experiment.

### Signaling assays

Intracellular cAMP was determined by homogenous time-resolved fluorescence (HTRF) (cAMP Dynamic 2 (CisBio) or LANCE® *Ultra* cAMP assay (PerkinElmer). In STC-1, HEK 293 cells or colonic crypts, cultures were pre-treated with IBMX (Sigma, 0.5 mM, 5 min) prior to ligand stimulation (5 min) and lysed with lysis buffer 4 (CisBio). The lysates were centrifuged at 12,000 x g for 10 mins and the supernatants were transferred to white 384-well plates. Anti-cAMP-Cryptate donor and cAMP-d2 acceptor were added to the wells and HTRF was measured using the PHERAstar (FSX) plate reader (BMG Labtech) equipped with 340 excitation filter and 620 nm (donor and 665 (acceptor) emission filter. For Flp-In TREx HEK 293 FFA2-eYFP cells, cells were detached, re-suspended in a freshly prepared stimulation buffer (5mM HEPES, 0.5 mM IBMX (Sigma), 0.1% BSA in Hank's Balanced Salt Solution at pH 7.4) and transferred to OptiPlate™-384 microplates (PerkinElmer) prior to ligand stimulation (30 min). EucAMP tracer and ULight-anti-cAMP solutions were added to the cells and incubated for 1h. Plates were read using an EnVision® Multimode Plate Reader (PerkinElmer) with a UV2 320 excitation filter and two emission filters (203 Eu 615 and 205 APC 665). Measurement of IP<sub>1</sub> was carried out using HTRF (IP-one (CisBio) by incubating cells or colonic crypts with ligands in serum free media supplemented with 50 mM LiCl (2h). Following stimulation, cultures were lysed with lysis buffer 4 (CisBio) supplemented with 50 mM LiCl and centrifuged at 12,000 x g for 10 mins and the supernatants were transferred to white 384-well plates. Anti-IP<sub>1</sub>-Cryptate donor and IP<sub>1</sub>-d2 acceptor were added to the wells and HTRF was measured using the PHERAstar (FSX) plate reader. cAMP and IP<sub>1</sub> concentrations determined by CisBio were corrected for protein levels. Calcium mobilization was measured by Fluo4-AM Direct Calcium Assay Kit (Invitrogen). Cells or colonic crypts were incubated with calcium dye in phenol red and serum free media for 30 min at 37°C and then at room temperature for 30 min. Cells or colonic crypts were imaged live using Leica SP5 confocal microscope using a 20X dry objective and a 488nm excitation laser. Movies were recorded at 1 frame per second for 1 min prior to ligand addition and a further 5-10 min following ligand addition to allow for calcium levels to lower to basal. The human phospho-kinase array kit (R&D system) containing 46 phosphokinases printed in duplication was used to identify a signaling pathway. STC-1 cells were serum-starved for 2 h prior to ligand stimulation and then lysed with array lysis buffer. Cell lysates were centrifuged at 12,000 x g for 10 min and protein concentrations were determined using Coomassie (Bradford) protein assay (Pierce). Protein lysates were incubated with the antibody-array membrane overnight and was then incubated with cocktail-detection antibody and streptavidin horseradish peroxidase. Protein signals were detected by the array Chemireagent and exposed to autoradiography film (GE healthcare). Spot intensity was quantified with ImageJ. For the measurement of p38 activation by western blot, STC-1 cells were serum-starved for 2 h prior to ligand stimulation. Following ligand stimulation, cells were rapidly washed with cold PBS and harvested with lysis buffer (1% Triton X-100, 50 mM Tris-HCl (pH 7.4), 150 mM NaCl, 0.5 mM EDTA, 1 mM NaF, 1 mM NaVO<sub>3</sub> and a protease inhibitor tablet (Roche)). Cell lysates were centrifuged at 12,000 x g for 10 min and protein concentrations were determined using Coomassie (Bradford) protein assay. Protein lysates were denatured at 95°C for 5 min in lysis buffer and Laemmli loading buffer containing 2% β-mercaptoethanol and separated on a 12% Tris-glycine polyacrylamide gel and transferred to nitrocellulose membranes. Membranes were incubated overnight with anti-rabbit phospho-p38 MAPK antibody (9211, Cell Signalling, 1/500) or anti-rabbit p38 MAPK antibody (9212, Cell Signalling, 1/1000) as a loading control. Specific protein bands were visualized using the ImageQuant Las 4000 chemi-image (GE Healthcare) and Luminata Forte HRP substrate (Millipore). Densitometry of the bands were quantified with ImageJ. Pre-treatments with either Ptx (Tocris), YM-254890 (Wako), Dyngo-4A (Abcam) or SB 203580 (Abcam) were carried out by incubating cells or colonic crypts for 20 h with 200 ng/mL Ptx, 5 min with 10 μM YM-254890, 45 min with 50 μM Dyngo-4a or 10 min with 5 μM SB 203580 before the addition of ligands. Experiments were conducted in duplicates for calcium mobilization and triplicates for all other experiments and were repeated at least three times.

### Western blot

To determine total cellular levels of β-ARR 1/2 and APPL1, cells were lysed with lysis buffer (1% Triton X-100, 50 mM Tris-HCl (pH 7.4), 150 mM NaCl, 0.5 mM EDTA, 1 mM NaF, 1 mM NaVO<sub>3</sub> and a protease inhibitor tablet (Roche)). Cell lysates were centrifuged at 12,000 x g for 10 min and protein concentrations were determined using Coomassie (Bradford) protein assay. Protein lysates were denatured at 95°C for 5 min in lysis buffer and Laemmli loading buffer containing 2% β-mercaptoethanol and separated on a 12% Tris-glycine polyacrylamide gel and transferred to nitrocellulose membranes. Membranes were incubated overnight either with anti-rabbit β-ARR 1/2 (3858, Cell Signalling, 1/1000) or anti-rabbit APPL1 (3858, Cell Signalling, 1/400) and then with anti-mouse GAPDH antibody (AB2302, 1/10,000, Millipore) as a loading control. Specific protein bands were visualized using the ImageQuant Las 4000 chemi-image (GE Healthcare) and Luminata Forte HRP substrate (Millipore).

### GLP-1 secretion assays

Plated STC-1 cells and colonic crypts were washed with secretion buffer (HBSS supplemented 1% BSA fatty acid free, which was adjusted to pH 7.4 with NaOH) and incubated in secretion buffer containing ligands for 2 h for STC-1 cells and 1 h for colonic crypts at 37°C. Inhibitors were used as for signaling assays. Following incubation, cell supernatants were collected, and the cells were lysed with lysis buffer (0.25 g sodium deoxycholate monohydrate, 0.88g NaCl, 0.5mL Igepal, 80 mM Tris HCL, pH 8, 1 tablet of complete EDTA-free protease cocktail inhibitor (Roche)). Samples were analyzed for GLP-1 secretion via an established in-house radioimmunoassay



(Kreyman et al., 1987) using the NE1600 $\gamma$  scintillation counter (Thermo Electron Corporation). The GLP-1 antibody has 100% cross-reactivity with all amidated forms of GLP-1 but does not cross-react with glycine extended forms. The intra-assay coefficients of variation for GLP-1 were 5.6%. As a control of GLP-1 release in the presence of inhibitors, cells or colonic crypts in the absence of inhibitors that secreted GLP-1 equivalent or less than NaCl were excluded from further analysis. All experiments were conducted in duplicate for colonic crypts and triplicate for STC-1 cells and repeated at least 3 times.

### Flow cytometry

Flow cytometry was used to quantitate internalization of FFA2 by measuring levels of receptor loss from the surface. Cells were fed live with M1 anti-FLAG antibody (20 min, 37°C) prior to treatment with ligands. Cells were then washed, lifted with PBS containing 2% FBS, centrifuged, and cell pellet washed with PBS and incubated with Alexa Fluor 488 secondary antibody (1h, 4°C). The fluorescence intensity of 10,000 cells were collected for each treatment and performed in triplicate using a FACS Calibur flow cytometer (BD Biosciences). Cells that were not exposed to any antibodies or secondary antibody alone were used for controls. All experiments were conducted at least three times.

### Immunofluorescence and confocal imaging

Receptor imaging in live or fixed cells were conducted by incubating live cells with FLAG M1-antibody (F3040, Sigma, 1/500) (20 min, 37°C) and then with fluorescent secondary antibody (20 min, 37°C for live cell imaging) in phenol-red-free DMEM prior to agonist treatment. If inhibitors were used these were administered to the cells at appropriate time before ligand stimulation. To fix cells, cells were washed three times in PBS/0.04% EDTA to remove FLAG antibody bound to surface receptors prior to fixation with 4% paraformaldehyde in PBS (20 min), blocked with 2% FBS (1 h), permeabilized using 0.2% TritonX100, incubated with either anti-rabbit EEA1 (3288, Cell Signalling, 1/400) or APPL1 (3858, Cell Signalling, 1/400) for 1 h, washed and subsequently incubated with goat anti-mouse or rabbit Alexa Fluor secondary antibodies (Invitrogen) (1 h) at RT. Cells were washed again and mounted with Fluoromount-G (Thermo Fisher). Both live and fixed cells were visualized via a TCS-SP5 microscope (Leica) with a 63x oil-immersion objective and 1.4 numerical aperture (NA). Images were acquired using Leica LAS AF image acquisition software. Raw-image file were analyzed using ImageJ or LAS AF Lite (Leica) to measure endosomes diameter size or level of co-localization.

### TIRFM

Cells were imaged using the Elyra PS.1 AxioObserver Z1 motorized inverted microscope with a sCMOS or EMCCD camera and an alpha Plan-Apochromat 100x/1.46 Oil DIC M27 Elyra objective (Zeiss), with solid-state lasers of 488 nm, 561 nm and/642 nm as light sources. For live cell imaging, approximately 15 minutes prior to imaging, culture media was replaced with Opti-MEM reduced serum media supplemented with HEPES. Imaging was then carried out using a Zeiss Elyra PS.1 microscope controlled at 37°C with 5% CO<sub>2</sub>. Time-lapse movies of whole cells were taken for 60 seconds, at 10 frames per second (fps) using Zen lite acquisition software. Fixed cells were prepared as for confocal imaging.

### Statistical analysis

Data are represented as mean  $\pm$  SEM. Mann-Whitney t-test, one-way ANOVA followed by Dunnett's post-test, or two-way ANOVA followed by Bonferroni post-test was used when comparing two groups, more than two groups or at least two groups under multiple conditions, respectively. Statistical significance was determined using GraphPad Prism. The number of samples (n) has been indicated for each figure panel. Differences were considered significant  $p \leq 0.05$ .

### Supplemental References

- Hoveyda, H. R., Fraser, G. L., Zoute, L., Dutheil, G., Schils, D., Brantis, C., Lapin, A., Parcq, J., Guitard, S., Lenoir, F., et al. (2018). N-Thiazolylamide-based free fatty-acid 2 receptor agonists: Discovery, lead optimization and demonstration of off-target effect in a diabetes model. *Bioorg Med Chem*, 26, 5169-5180.
- Kreyman, B., Williams, G., Ghatei, M. A. & Bloom, S. R. (1987). Glucagon-like peptide-1 7-36: a physiological incretin in man. *Lancet*, 2, 1300-4.
- Maslowski, K. M., Vieira, A. T., Ng, A., Kranich, J., Sierro, F., Yu, D., Schilter, H. C., Rolph, M. S., Mackay, F., Artis, D., et al. (2009). Regulation of inflammatory responses by gut microbiota and chemoattractant receptor GPR43. *Nature*, 461, 1282-6.
- Olken, N. M. & Marletta, M. A. (1992). NG-allyl- and NG-cyclopropyl-L-arginine: two novel inhibitors of macrophage nitric oxide synthase. *J Med Chem*, 35, 1137-44.
- Roman, G., Vlahakis, J. Z., Vukomanovic, D., Nakatsu, K. & Szarek, W. A. (2010). Heme oxygenase inhibition by 1-aryl-2-(1h-imidazol-1-yl)/1h-1,2,4-triazol-1-yl)ethanones and their derivatives. *ChemMedChem*, 5, 1541-55.